Title page

Title

naRNA is a canonical neutrophil extracellular trap (NET) component and novel inflammation-amplifying composite DAMP

Running title

naRNA – canonical NET component and composite DAMP

Authors

Francesca Bork[1], Carsten L. Greve[1], Christine Youn[2], Sirui Chen[1], Yu Wang[2], Masoud Nasri[3], Jule Focken[4], Jasmin Scheurer[4], Pujan Engels[1], Marissa Dubbelaar[1,5], Katharina Hipp[6], Birgit Schittek[4,7,8], Stefanie Bugl[1], Markus W. Löffler[1,7,9], Julia Skokowa[3,7], Nathan K. Archer[2] (ORCID: 0000-0002-8212-8985), Alexander N.R. Weber[1,7,8]* (ORCID: 0000-0002-8627-7056)

Author information

[1]Interfaculty Institute for Cell Biology, Department of Immunology, University of Tübingen, Auf der Morgenstelle 15, 72076 Tübingen, Germany

[2]Department of Dermatology, Johns Hopkins University School of Medicine, Baltimore, MD 21231, USA

[3]Division of Translational Oncology, Department of Oncology, Hematology, Clinical Immunology and Rheumatology, University Hospital Tübingen, Otfried-Müller Str. 10, 72076 Tübingen, Germany

[4]Division of Dermatooncology, Department of Dermatology, University Hospital Tübingen, Liebermeisterstr. 25, 72076 Tübingen, Germany

[5]Quantitative Biology Center (QBiC), University of Tübingen, Auf der Morgenstelle 10, 72076 Tübingen, Germany

[6]Electron Microscopy Facility, Max Planck Institute for Biology Tübingen, Max-Planck-Ring 5, 72076 Tübingen, Germany

[7]iFIT – Cluster of Excellence (EXC 2180) "Image-Guided and Functionally Instructed Tumor Therapies", University of Tübingen, Germany

[8]CMFI – Cluster of Excellence (EXC 2124) "Controlling microbes to fight infection", University of Tübingen, Germany.

[9]Department of General, Visceral and Transplant Surgery, University Hospital Tübingen, Hoppe-Seyler-Str. 3, 72076 Tübingen, Germany and Department of Clinical Pharmacology, University Hospital Tübingen, Auf der Morgenstelle 8, 72076 Tübingen, Germany

Corresponding Author

Alexander N. R. Weber, Interfaculty Institute for Cell Biology, Department of Immunology, University of Tübingen, Auf der Morgenstelle 15, 72076 Tübingen, Germany. Tel.: +49 7071 29 87623. Fax: +49 7071 29 4579. Email: alexander.weber@uni-tuebingen.de; ORCID: 0000-0002-8627-7056, Twitter @aweberlab

Abstract

Neutrophil extracellular traps (NETs) have emerged as a key feature of cellular innate immunity mediated by polymorphonuclear neutrophils (PMNs), the primary leukocyte population in humans. Forming web-like structures composed of DNA, histones, and antimicrobial proteins, NETs trap and kill microbial invaders and thus enhance host defense. However, they have also been linked to inflammatory states, e.g. in atherosclerosis or psoriasis. Whilst DNA has been in focus as a primary structural component of NETs, we here characterize naRNA (NET-associated RNA), as a new canonical, abundant, and largely unexplored NET component. naRNA decorated all types of NETs in complex with the antimicrobial peptide LL37. In fact, naRNA was pre-associated with LL37 intracellularly as a 'composite' danger-associated molecular pattern (DAMP) prior to neutrophil activation. Externalized, naRNA propagated NET formation in naïve PMN, dependent on TLR8 in humans and Tlr13 in mice, in vitro and in vivo. naRNA-TLR8/Tlr13 signaling contributed significantly to the highly sensitive pro-inflammatory response of both tissue cells, like keratinocytes, and other immune cell types, such as macrophages. Those responses could be blocked by inhibition and genetic ablation of RNA receptors or RNase treatment. Importantly, in vivo naRNA strongly drove skin inflammation whereas genetic ablation of RNA sensing drastically ameliorated skin inflammation in the imiquimod psoriasis model. Our data highlight naRNA as a novel composite DAMP signaling and amplifying neutrophil activation. Moreover, naRNA emerges as the likely driver of inflammation in conditions previously linked to NETs and extracellular RNA, suggesting blockade of TLR-mediated RNA sensing as potential new intervention target.

Graphical abstract

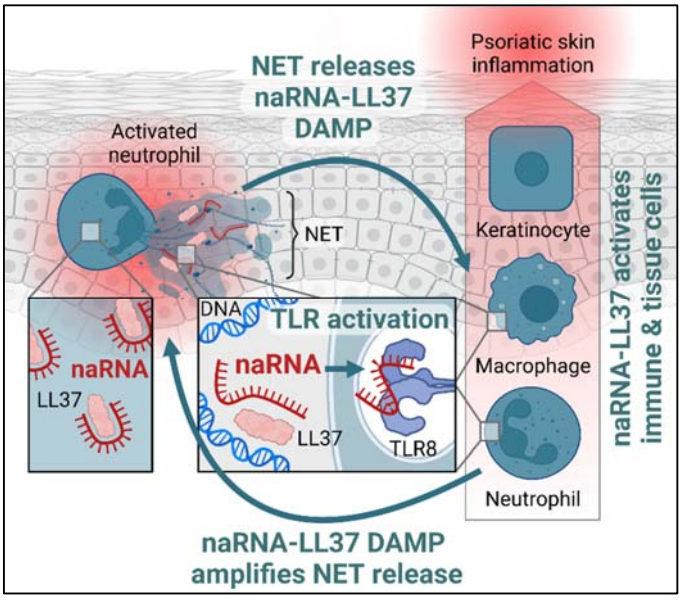

Created with biorender.com

Introduction

The formation of Neutrophil Extracellular Traps (NETs), since its discovery in 2004 (Brinkmann, Reichard et al. 2004), has emerged as a fascinating phenomenon of host defense. Hereby neutrophils, the primary leukocyte population, extrude their genomic DNA to form web-like structures that, similar to barbed wire roadblocks, trap and kill microbial invaders such as bacteria or fungi (Kruger, Saffarzadeh et al. 2015). DNA is thus a defining structural and functional feature of NETs. Additionally, DNA-associated proteins, histones and HMGB-1, antimicrobial peptides like LL37 and enzymes such as myeloperoxidase (MPO) are released during the formation of NETs and contribute to their antimicrobial function (Kruger, Saffarzadeh et al. 2015). More than 1,000 publications on NETs have sought to detail the multi-faceted phenomenon and the processes that lead to its execution (Boeltz, Amini et al. 2019). However, with the main focus devoted to DNA and protein components, another primary cellular biomolecule, RNA, has so far received very little attention in vertebrates. Interestingly, a study in insects showed that, hemocytes (macrophage-like immune cells) can release both DNA and RNA in NET-like structures during microbe-triggered clotting reactions, and in response to extracellular RNA or DNA (Altincicek, Stotzel et al. 2008). Our lab recently provided evidence of a responsiveness of human polymorphonuclear neutrophils (PMNs) to RNA, but not DNA, in combination with the antimicrobial peptide LL37, fueling neutrophil activation (Herster, Bittner et al. 2020). In addition, earlier work described a role for DNA- and RNA-LL37 complexes in the activation of plasmacytoid dendritic cells (Lande, Gregorio et al. 2007, Ganguly, Chamilos et al. 2009). This has given rise to the notion that under certain conditions tolerance to self-DNA and RNA can be broken involving the nucleic acid-sensing TLR7, TLR8 (ssRNA) and TLR9 (DNA) in humans and Tlr7, Tlr13 and Tlr9 in mice. In general, many roles have been ascribed to so-called extracellular RNA (exRNA), for example, macrophage polarization, recruitment of leukocytes to the site of inflammation, leukocyte rolling at the vascular endothelium, as well as integrin-mediated firm adhesion of immune cells and promotion of thrombosis (Preissner, Fischer et al. 2020). Additionally, exRNA is considered as a reliable biomarker for various diseases such as cancer or cardiovascular pathologies (Schmidt, Engel et al. 2005, Zernecke and Preissner 2016). However, RNA being considered a short-lived biomolecule, physiological sources of exRNA have been somewhat unclear. Under sterile conditions, vascular injury, tissue damage, or ischemia have been suggested to trigger release of exRNA along with other cellular material (Preissner, Fischer et al. 2020). However, it remains unclear whether these relatively slow processes could amount to physiologically detectable exRNA amounts in the serum of patients, or whether a rapid, as-yet unidentified process of RNA extrusion would have to be postulated.

We speculated that RNA contained in NETs, so-called NET-associated RNA or naRNA, might lead to a feed-forward loop of rapidly expanding NET release amongst neutrophils which might also engulf

additional tissue or immune cells able to respond to exRNA. We show here that naRNA drives such a self-amplifying loop not only engaging PMN but also macrophages, and keratinocytes. naRNA responsiveness was dependent on *TLR8* and *Tlr13* in human and murine myeloid immune cells, respectively. Interestingly, naRNA appears pre-complexed to LL37 as a novel composite DAMP. Notably, in mice naRNA caused considerable skin inflammation in a Tlr13-dependent manner. Additionally, in a well-established model of psoriatic skin inflammation, genetic ablation of RNA sensing strongly ameliorated skin inflammation, highlighting naRNA as a potent damage associate molecular pattern (DAMP) amplifying PMN activation and alerting tissue and other immune cells.

Results

naRNA is a common component of NETs

To first identify whether naRNA was a common component of NETs, we compared NETs from human PMN formed in response to the well-defined molecular agonists PMA, different complexes of LL37 with purified RNA (synthetic, as well as total fungal and bacterial RNA from *S. aureus* and *C. albicans*, respectively), nigericin (Munzer, Negro et al. 2021) and the live pathogen *C. albicans*. Confocal microscopy analysis using the well-characterized rRNA-specific antibody, Y10b (Lerner, Lerner et al. 1981), revealed the presence of RNA in all corresponding NETs, independent of stimulus and whether NET formation was suicidal or not (Fig. 1A, quantified in B; control in Fig. S1A): the RNA signal was readily detectable along the web-like DNA threads in human NETs. Similar results were obtained in NETs released by murine bone marrow-derived PMN (BM-PMN, Fig. 1C; control Fig. S1B). To avoid the use of staining reagents, we also metabolically labeled primary human hematopoietic stem cells (HSCs) with 5-ethynyluridine (5-EU), a nucleotide that can be incorporated in cellular RNA but not DNA, and that is amenable to labeling by click chemistry (Presolski, Hong et al. 2011). These HSCs were then differentiated to neutrophils (Sioud 2020) and the differentiation validated by microscopy and flow cytometric analysis (Fig. S1C, D). NETs released from HSC-derived PMN could indeed be labeled with click reagents conferring a fluorescent label only when grown in 5-EU-containing medium (Fig. 1D). Moreover, the overlap between click-label and rRNA confirmed the specificity of the staining with anti-rRNA antibodies and indicated that naRNA contained rRNA but also other types of cellular RNAs. This experiment also unequivocally confirmed that upon PMN stimulation, cellular RNA is turned into a component of the NET, wherein it decorates the fine, web-like DNA structures. The localization of naRNA on DNA strands was further confirmed by high-resolution fluorescence microscopy and 3D analysis (AiryScan, Fig. 1E and Supplemental Movie S1) as well as scanning electron microscopy (SEM, Fig. 1F; controls Fig. S1E). Extraction of naRNA from PMA-induced NETs (Fig. 1G) and subsequent RNA-sequencing analysis confirmed that purified naRNA contained multiple RNA types, with noticeably more non-ribosomal RNA than the corresponding total cellular RNA of PMNs (Fig. 1H). Collectively,

these results indicate that naRNA is a canonical component of NETs released upon multiple stimuli from both human and murine neutrophils.

naRNA is a potent DAMP propagating NET formation in primary PMN

A primary function of NETs is host defense by trapping and killing bacteria. Therefore, we first explored if naRNA participated in this process (Brinkmann, Reichard et al. 2004). However, the antibacterial effect of NETs on live *Staphylococcus aureus* (evidenced by lower CFUs compared to resting PMNs) was similar to that of RNase-treated NETs, whereas DNase digestion reduced the drop in CFU discernibly but non-significantly (Fig. S2A). Consequently, we turned our attention to a possible role of naRNA as a DAMP, since primary PMN can respond to synthetic RNA-LL37 complexes with NET formation, and our analysis indicated that NETs also contain LL37 (Herster, Bittner et al. 2020). To prepare a naRNA-containing stimulant, PMA-induced NETs were prepared as described in Methods and the original stimulus, PMA, removed by extensive washing before harvesting. Interestingly, these 'PMA NETs', when applied to naïve PMN from another donor, potently induced new NETs (Fig. 2B, quantified in C, controls in Fig. S2B). Treatment with an RNase inhibitor enhanced the stimulatory effect of PMA NETs rendering a 1:500 dilution of PMA-NETs more effective than a 1:50 dilution of non-treated PMA-NETs (Fig. 2B, C, controls Fig. S2B). Interestingly, similar NET preparations from mock-treated PMNs (here referred to as 'mock NETs') did not stimulate NET formation under the same experimental conditions. To rule out the possibility that residual PMA in PMA NETs could be responsible for the observed stimulatory effects, RNase treatment was also performed which strongly reduced NET formation (Fig. 2D, quantified in E; controls Fig. S2C). Interestingly, DNase digestion had the same effect as RNase treatment, probably because digestions/removal of the DNA scaffold would cause a loss of associated naRNA (*cf.* Fig. 1E). This was also confirmed by rapid loss of the RNA signal (using the RNA-selective dye, SYTO RNAselect (Herster, Bittner et al. 2020) in time-lapse digestion analysis of DNA digestions (Supplemental Movie S2 and S3). Bearing in mind that PMNs do not respond to DNA or DNA-LL37 complexes (Herster, Bittner et al. 2020), the opposing effects of RNase inhibitor and RNase treatments thus clearly indicated naRNA (and not DNA) to be the relevant immunostimulatory component for NETs to drive the activation of naïve PMN. In line with our previous work showing that synthetic RNA or LL37 alone cannot trigger PMN activation (Herster, Bittner et al. 2020), purified 'naked' naRNA isolated from PMA NETs (*cf.* Fig. 1G) was unable to activate NET formation; however, re-complexing with exogenous LL37 was sufficient to restore NET formation (Fig. 2F, controls in Fig. S2D). We next investigated whether in NETs, naRNA co-localized with LL37. Strong co-localization was evident in confocal microscopy analysis (Fig. 2G) and confirmed by Pearson's colocalization analysis (Fig. 2H). Additional line plot analysis of PMA-stimulated PMN revealed that RNA and LL37 did in fact co-localize in NETs, i.e., after extrusion (Fig. S2E). Surprisingly, in unstimulated PMNs naRNA and LL37 showed even greater colocalization (Fig. 2H), suggesting pre-association before

extrusion (Fig. S2E). The concept of pre-packaging also fits with the RNAseq data showing that certain RNA types are lost upon release (*cf.* Fig. 1H), probably because they are not bound to LL37. Collectively, naRNA appears to be LL37-pre-associated, and hence a 'composite' DAMP, enabling PMN activation and NET propagation.

naRNA DAMP activity is dependent on RNA sensors TLR8/Tlr13

To validate naRNA as an immunostimulatory RNA component from the receptor side, we turned to HEK293T cells which do not respond to RNA, unless transfected with plasmids encoding the human ssRNA sensors TLR7 or TLR8 (Colak, Leslie et al. 2014). NF-κB reporter assays revealed that TLR7 or TLR8- but not TLR9 (a human DNA sensor)-transfected HEK293T cells stimulated with PMA NETs or mock NETs showed robust NF-κB activity only for PMA NETs (Fig. 3A). R848 (TLR7 and TLR8 agonist) and TL8 or ssRNA+DOTAP (TLR8 agonist) served as controls. Of note, compared to its cognate agonist CpG, the DNA sensor TLR9 was only poorly activated by PMA NETs, indicating that naRNA is a superior immune stimulant compared to NET DNA in this system. Indeed, the observed response of primary PMNs (Fig. 3B, quantified in C; in Fig. S3A) could be completely blocked by the TLR8-specific inhibitor, CU-CPT9a (Zhang, Hu et al. 2018), similar to the effects of the PAD4 inhibitor, Cl-amidine (Fig. 3C and S3A). This revealed the RNA sensor TLR8 (Heil, Hemmi et al. 2004) to be the naRNA receptor in primary human PMNs. We further genetically validated the involvement of RNA sensing in naRNA-mediated NET propagation using BM-PMN from *Unc93b1*- or *Tlr13*-defective mice: whereas in *Unc93b1*-defective mice signaling of all endosomal TLRs is abrogated (Tabeta, Hoebe et al. 2006), mice lacking *Tlr13,* the murine equivalent of TLR8 (Eigenbrod and Dalpke 2015), specifically lack ssRNA sensing (Li and Chen 2012), respectively. Confocal microscopy analysis showed that WT BM-PMN responded readily to both PMA (used as control) and PMA NETs, whereas *Unc93b1* (Fig. S3B) or *Tlr13* KO PMN (Fig. 3D, quantified in E) only responded to the TLR-independent PMA control but not PMA NETs. This receptor analysis unequivocally confirmed naRNA to be a primary immune stimulant in NETs.

PMN-derived naRNA triggers broader immune cell and keratinocyte activation

Given the potent effect of naRNA on naïve PMNs (*cf.* Fig. 3B-E) and the ability of human macrophages to sense RNA via TLR8 (Ishii, Funami et al. 2014), we hypothesized that naRNA might also directly activate macrophages, which are rapidly recruited at the sites of PMN activation in peripheral tissues (Mahdavian Delavary, van der Veer et al. 2011), contributing to an inflammatory process in vivo. We thus assessed the effects of naRNA on genetically modified macrophage-like cell lines: BlaER1 macrophages (Vierbuchen, Bang et al. 2017) responded to PMA NETs but not mock NETs with IL-8 release, and this was TLR8-dependent as evidenced by comparisons of WT and *TLR8*-edited BlaER1 cells (Fig. 3F). Use of a naRNA-stabilizing RNase inhibitor during NET preparation (*cf.* Fig. 2B) drastically increased the potency of PMA NETs on these macrophages. Additionally, TLR8 and TLR7-edited THP-1

macrophage-like cells (Coch, Hommertgen et al. 2019) responded to PMA NETs with lower relative IL-8 release than WT THP-1 cells (Fig. S4A), confirming RNA as the active agent in monocyte/macrophage activation. Human peripheral blood mononuclear cells (PBMCs) were also stimulated with different NET preparations. RNA-stabilized PMA NETs consistently elicited higher TNF, IL-6 and IL-8 levels than non-stabilized PMA- or mock NETs (Fig. S4B-D). However, this effect was not sensitive to the TLR8 inhibitor Cu-CPT9a, which is consistent with the ability of TLR7 to also sense naRNA (*cf.* Fig. 3A) and possibly due to a mixture of cells being present. Further analysis revealed that the natural killer (NK) cell line NK-92 MI showed low IFNγ release in response to RNA-stabilized PMA NETs (Fig. S4E). Collectively, our results show that the RNA component of NETs, naRNA, can engage not only bystander neutrophils in a feed-forward inflammatory response but also other myeloid (monocytes/macrophages) and lymphoid (NK cells) cellular innate immunity. To investigate whether non-hematopoietic cells with immune functions, e.g. tissue cells like keratinocytes, could also respond to RNA-stabilized PMA NETs, N/TERT-1 keratinocytes (Dickson, Hahn et al. 2000) in monolayers were exposed to PMA-NETs (Fig. 3G). This triggered a dose-dependent IL-8 release comparable to synthetic RNA+LL37, especially under RNA stabilization by RNase inhibitors. Similar results were obtained using primary normal human epidermal keratinocyte (NHEK) monolayers (Fig. 3H). Furthermore, in an 'in vivo'-like human skin equivalent 3D model in which natural keratinocyte differentiation was recapitulated by NHEK cells (Bitschar, Sauer et al. 2019)), PMA but not mock NETs significantly induced *IL8* mRNA and protein (Fig. 3I, J). Thus, naRNA can not only activate primary neutrophils in vitro but also trigger broad immune activation in other immune and tissue cells/equivalents.

naRNA displays DAMP activity in vivo in dependence on RNA sensing

Finally, to gain an insight into whether naRNA could trigger inflammation in vivo in an RNA receptor-dependent manner, we intradermally injected RNase inhibitor-stabilized mock or PMA NETs in the ears of C57BL6 mice. RNA-stabilized PMA NETs were almost as potent to induce ear swelling as synthetic RNA+LL37 (Fig. 4A), but even non-stabilized PMA NETs induced a response significantly higher than mock NETs. The same stimulants were also injected into the ear of *LysM*$^{EGFP/+}$ mice, in which myeloid cells are GFP-positive, thus enabling in vivo monitoring of cellular influx during skin inflammation. Here, RNA-stabilized PMA NETs elicited even greater cellular influx than synthetic RNA+LL37 and mock NETs (Fig. 4B). Importantly, a comparison of WT and *Tlr13*-deficient animals showed that the ear swelling reaction resulting in vivo was naRNA-dependent because RNA-stabilized PMA-NETs were significantly less effective in *Tlr13*-deficient animals (Fig. 4C).

Self-RNA recognition contributes to progressive skin inflammation in experimental psoriasis

Finally, we sought to explore if naRNA was relevant in an animal disease model. The most frequently used murine model of psoriasis uses the TLR7 ligand imiquimod (IMQ) to trigger increasing skin

inflammation characterized by epidermal thickening and immune cell infiltration. We previously showed that IMQ treatment also leads to the occurrence of NETs in the tissue (Herster, Bittner et al. 2020). We therefore speculated that naRNA might be involved in disease progression, a hypothesis that could be probed by genetically ablating naRNA sensing and comparing WT and *Tlr13* KO mice. Although in the early induction phase, WT and *Tlr13* KO animals showed a similar increase in ear thickness, the groups diverged from day 3 onwards, after which *Tlr13*-deficient animals were significantly protected from skin inflammation compared to WT mice (Fig. 4D). The most plausible explanation is that IMQ-initiated NET formation (Herster, Bittner et al. 2020) amplifies skin inflammation in WT animals via naRNA, whereas this is prevented in *Tlr13* KO animals. This shows that naRNA can significantly contribute to inflammation in a well-established disease model and can act as a potent inflammation-amplifying endogenous DAMP.

Discussion

At first sight, it may not seem surprising that the release of NETs, a process that churns up the most critical compartment of a cell, e.g., the nucleus, also inevitably leads to the release of another primary cellular biomolecule, namely RNA. However, independently of whether the process is regulated or not, the release of RNA by NETting PMN appears to have physiological importance as we have demonstrated here. Rather than acting directly in antimicrobial defense (*cf.* Fig. S2A), naRNA appears to be an LL37-precomplexed DAMP of PMN origin that can be released in the NETting process and then activates both PMN and other immune and tissue cells in an RNA sensor-dependent manner (Fig. S5). Several further findings warrant further discussion:

Firstly, our data revise previous concepts of self-RNA and LL37 in the ‘breaking’ of innate immune tolerance in psoriasis and the physiological role of NETs in general: We found that only when naRNA is complexed with LL37, it gains stimulatory properties on neutrophils (*cf.* Fig. 2F), comparable to other RNAs tested so far. Based on earlier work (Herster, Bittner et al. 2020) (Kulkarni, O'Neill et al. 2021), LL37 thus may function as a physiological ‘transfection reagent’ of naRNA mediating its uptake into immune cells, but possibly also shielding it from RNase degradation. LL37 thus moonlights as an immunomodulatory peptide rather than only possessing antimicrobial activities. However, RNA and LL37 do not appear to aggregate and co-localize ‘accidentally’ in NETs: quite unexpectedly, they were rather found in even greater co-localization in resting neutrophils, indicating a kind of ‘pre-association’ and intracellular storage of a pre-defined naRNA-LL37 ‘composite’ DAMP before extrusion during NET formation. Importantly, the identification of such pre-association challenges existing concepts of LL37-RNA complexes as ‘accidentally assembled’ tolerance breakers in certain diseases (Ganguly, Chamilos et al. 2009). Rather, it suggests naRNA-LL37 complexes act as ‘purposefully pre-associated’ DAMPs that arm neutrophils. It will be interesting to study the process for pre-association for this first ‘composite

DAMP' and elucidate the precise nature of the RNAs assembled with LL37 in the future. Intracellular (rather than accidental/extracellular) pre-association points to a specific role of the naRNA-LL37 DAMP in NET biology. Beyond simply amplifying inflammation, we speculate that the physiological relevance of deploying this composite DAMP upon NET formation could be to tag fresh NETs with a timed molecular beacon: Freshly extruded NETs decorated with the naRNA-LL37 DAMP would likely highlight the lingering presence of a pathogenic microorganism or acute tissue damage to other cells not directly engaged by the threat. The naRNA-LL37 DAMP would thus label 'fresh NETs' as 'requiring attention' and triggering further immune activation. Over time, whilst the DNA-related structural and antimicrobial properties of NETs may remain longer, inevitable RNA degradation would lead to deactivation of the composite DAMP, rendering 'old NETs' less immunostimulatory. Further work outside the scope of the present study may explore such a role of naRNA as time-restricted molecular label for NETs.

Moreover, our data pertain to the origin and effects of 'extracellular RNA' (exRNA). exRNA is a generic term to indicate a heterogeneous group of RNA molecules which are actively or passively released during sterile inflammation or infectious processes. exRNA can be released in a 'free' state, bound to proteins or phospholipids, in association with extracellular vesicles (EVs) or apoptotic bodies (Preissner, Fischer et al. 2020). In all these forms exRNA may function as DAMP but also as e.g., procoagulant or regenerative factor (Preissner, Fischer et al. 2020). Our data identify naRNA as the first type of exRNA for which a clear physiological origin (NETs) is provided. We speculate that our findings will help trace multiple descriptions of exRNA on the one side, to neutrophil ETs on the other. For example, exRNA has emerged as disease-relevant in atherosclerosis, where it was described to act as a proinflammatory mediator enhancing the recruitment of leukocytes to the site of atherosclerotic lesions as shown in a mouse model of accelerated atherosclerosis (Simsekyilmaz, Cabrera-Fuentes et al. 2014). At the same time, NETs have been ascribed a role in amplifying sterile inflammatory responses in an independent mouse model of atherosclerosis by priming macrophages (Warnatsch, Ioannou et al. 2015). However, never have these two independent strains of research been connected. By showing NETs to release naRNA, a type of exRNA, our work connects both lines of enquiry. Likewise, for rheumatoid arthritis (RA), our work makes a plausible link between exRNA in synovial fluid contributing to joint inflammation (Neumann, Hasseli et al. 2018), the emerging role of NETs in RA (Song, Ye et al. 2020) and even a hitherto enigmatic but therapeutically relevant role of TLR8 (Sacre, Lo et al. 2008, Sacre, Lo et al. 2016). We suspect similar links to emerge for cardiovascular diseases and cancer if the role of naRNA is thoroughly assessed. Furthermore, the broad sensitivity of immune and tissue cells to naRNA observed by us makes sense of how exRNA may act pathophysiologically.

Although we believe PMN to be the primary trap forming human leukocyte population and hence naRNA the most significant "trap-associated RNA", it will be interesting to explore whether mast cell

(MCETs) (Mollerherm, von Kockritz-Blickwede et al. 2016) or macrophage extracellular traps (METs) (Doster, Rogers et al. 2018) contain RNA. However, unlike PMN, the latter immune cells are not primary sources of LL37 (Sorensen, Arnljots et al. 1997), so that RNA associated with MCETs or METs would be of lesser physiological relevance as a DAMP than naRNA due to a lack of LL37. Therefore, translational approaches, e.g. to restrict trap-RNA mediated amplification of inflammation, should probably center on PMN-derived naRNA. The use of PAD4 inhibitors has already been investigated in animal models to treat cancer or atherosclerotic lesions (Li, Lin et al. 2020) (Knight, Luo et al. 2014) and would represent one potential way of eliminating NETs and hence naRNA-mediated inflammation. However, this would also prevent the effects of NETs that are beneficial for host defense (e.g. physical trapping via DNA and antimicrobial enzymatic activities) and may render treated patients vulnerable to infections. From a translational perspective, our in vivo data indicate that blockade of RNA sensing might be more advantageous, restricting only naRNA mediated responses. Although probably not applicable to patients, it is underscored by evidence that neuroinflammation upon subarachnoid hemorrhage, which is characterized by a NET pathology, is strongly ameliorated by RNase treatment in vivo (Fruh, Tielking et al. 2021). More applicable to patients may be the targeting of TLR8 by small molecular antagonists (Vlach, Bender et al. 2021) or inhibitory oligonucleotides, which are able to block PMN responsiveness to synthetic RNA in vitro (Herster, Bittner et al. 2020). Exciting is thus the observed efficacy of TLR inhibitory oligoribonucleotides in a psoriasis mouse model (Jiang, Zhu et al. 2013) and even a first clinical trial in psoriasis patients (Balak, van Doorn et al. 2017). We could imagine the blockade of naRNA effects via TLRs highlighted here to emerge as an effective novel strategy to target multiple exRNA or NET-related inflammatory responses.

Figure legends

Fig. 1: **naRNA is a canonical component of NETs.**

(A, B) Confocal microscopy of primary human PMNs stimulated as indicated for 3 h and stained for naRNA (anti-rRNA Y10b, magenta) and DNA (Hoechst 33342, white; n = 3, scale bar: 10 µm, arrowheads point to selected NET strands; representative images in **A**) were quantified in **B** (each dot represents one image, *p<0.05 according to one-way ANOVA). **(C)** Confocal microscopy of primary murine BM-PMNs stimulated as indicated for 16 h and stained as in **A** (n = 3, representative images, scale bar: 10 µm). **(D)** Confocal microscopy of primary human stem cells differentiated *in vitro* with/without 100 µM 5-ethynyl uridine (5-EU), click-labeled with a fluorescent dye (yellow, total RNA), anti-rRNA and Hoechst 33342 as in **A** (n = 3, representative images, scale bar: 10 µm, 2 µm in cropped image). **(E)** as in **A** but showing 3D image reconstruction of z-stacks (n = 3, representative images, scale bar: 10 µm). **(F)** Scanning electron microscopy of human primary PMNs treated as indicated and using anti-rRNA primary and immunogold (white arrow)-labeled secondary antibodies and silver enhancement (n = 3, representative images, scale bars as indicated; the two rightmost images show composite images with signals from secondary electron and backscattered electron detectors for topography and additional material information, respectively). **(G)** Agilent TapeStation quantification of naRNA isolated from mock or PMA NETs (from n = 4-6 donors, combined data, mean+SD, each dot represents one biological replicate/donor, *p<0.05 according to Mann-Whitney test). **(H)** RNAseq of PMA NET naRNA (n = 4) and whole PMN RNA (n = 1) (combined data).

Fig. 2. naRNA is a DAMP driving NET propagation in human PMN

(A) Workflow for NET content preparation from one donor and transfer to naïve human primary PMN from a second donor. **(B)** Confocal microscopy of primary human PMNs stimulated with NET content harvested with/without RNase inhibitor and diluted 1:50 or 1:500, and then stained for NETs/DNA (Hoechst 33342, n = 9, representative images, scale bar: 10 µm). **(C)** Quantification of **B** using DNA (Hoechst 33342) signal to quantify NET formation (n = 3, combined data, mean+SD, each dot represents one image, *p<0.05 according to one-way ANOVA). **(D)** as in **B** but with/without pre-digestion of NET content with RNase A or DNase I (n = 3, representative images; scale bar: 10 µm). **(E)** Quantification of **D** (n = 3, combined data, mean+SD, each dot represents the number of NET-positive tiles in one image quantified from three images/condition, *p<0.05 according to one-way ANOVA). **(F)** As in **B** but using purified naRNA (*cf.* Fig. 1G) alone or in complex with exogenously added LL37 (n = 3, representative images; scale bar: 10 µm). **(G)** Confocal microscopy of primary human PMNs stimulated as indicated for 3 h and stained for naRNA (anti-rRNA Y10b, magenta), LL37 (anti-hLL37-DyLight550, yellow), and DNA (Hoechst 33342, white; n = 3, representative images, scale bar 10 µm). **(H)** Pearson's

correlation coefficient (colocalization) analysis of **G** (n = 3, combined data, mean+SD, each dot represents one image, three images/condition, *p<0.05 according to one-way ANOVA).

Fig. 3. naRNA activity depends on RNA sensors

(A) NF-κB dual luciferase assay in HEK293T cell transiently transfected and stimulated as indicated (eV = empty vector, n=3-5, combined data, mean+SD, *p<0.05 according to one-way ANOVA). **(B)** Confocal microscopy of human primary PMNs stimulated as indicated in the presence or absence of CU-CPT9a (100 nM) or CI-amidine (200 µM, not shown) and stained for NETs/DNA (Hoechst 33342, white, n = 3, representative images, scale bar: 10 µm). **(C)** Quantification of **B** using DNA (Hoechst 33342) signal to quantify NET formation (n = 3, combined data, mean+SD, each dot represents the number of NET-positive tiles in one image, three images/condition, *p<0.05 according to non-parametric one-way ANOVA). **(D)** Confocal microscopy analysis of primary C57BL/6 WT or *Tlr13*$^{-/-}$ murine BM-PMNs stimulated as indicated and stained for NETs/DNA (Hoechst 33342, white, n = 3, representative images, scale bar: 10 µm). **(E)** Quantification of **D** as in **C** (n = 3, *p<0.05 according to one-way ANOVA. **(F)** Triplicate IL-8 ELISA from WT, *TLR8*$^{-/-}$ and *UNC93B1*$^{-/-}$ BlaER1 macrophage-like cells stimulated as indicated for 18 h (n = 2-3, combined data, mean+SD, each dot represents one biological replicate, *p<0.05 according to one-way ANOVA). **(G)** Triplicate IL-8 ELISA from N/TERT-1 keratinocytes stimulated as indicated for 24 h (n = 3, combined data, mean+SD, each dot represents one biological replicate, *p<0.05 according to one-way ANOVA). **(H)** as in G but with primary normal human epidermal keratinocytes (NHEK) (n = 3, combined data, mean+SD, each dot represents one biological replicate, *p<0.05 according to one-way ANOVA. **(I, J)** Triplicate relative (to unstimulated) *IL8* mRNA qPCR or IL-8 ELISA from NHEK 3D human skin equivalent constructs stimulated as indicated for 24 h (n = 2, representative of one biological replicate is shown, mean+SD, each dot represents one technical replicate, *p<0.05 according to one-way ANOVA).

Fig. 4. naRNA is a driver of NET-associated *in vivo* inflammation

(A) Ear thickness quantified daily in WT C57BL6 mice injected intradermally in vivo on day 0 as indicated (n = 5 per group, combined data, mean+SD, *p<0.05 according to two-way ANOVA). **(B)** Fluorescence imaging monitored hourly in *LysM*$^{EGFP/+}$ mice injected intradermally in vivo at t=0 as indicated (n = 10 per group, combined data, mean+SD, *p<0.05 according to two-way ANOVA). **(C)** As in **A** but also using *Tlr13*$^{-/-}$ mice (n = 7, combined data, mean+SD, *p<0.05 according to two-way ANOVA). **(D)** As in **C** but instead of intradermal injection with topical imiquimod application on day 0–4 (C57BL/6 n = 5, *Tlr13*$^{-/-}$ n = 3, combined data, mean+SD, *p<0.05 according to two-way ANOVA).

Fig. S1. Controls of IF microscopy, stem cell-derived PMNs, and electron microscopy

(A) Confocal microscopy of unstimulated primary human PMNs (control to Fig. 1A) after 3 h and stained for naRNA (anti-rRNA Y10b, magenta) and DNA (Hoechst 33342, white; n = 3, representative images,

scale bar: 10 µm). **(B)** Confocal microscopy of unstimulated primary murine BM-PMNs (control to Fig. 1C) after 16 h and stained as in **A** (n = 3, representative images, scale bar: 10 µm). **(C)** Brightfield microscopy analysis of cytospun control primary human stem cell-derived PMNs (control to Fig. 1D) differentiated *in vitro* with/without 100 µM 5-Ethynyluridine (5-EU, n = 3, representative images, scale bar: 20 µm). **(D)** FACS analysis for cells shown in **C** and Fig. 1D (n=3, representative data). **(E)** Scanning electron microscopy of PMA-treated human primary PMNs showing only secondary antibody staining (no primary antibody) control of Fig. 1F (n = 1, representative data; the image on the right is a composite image with signals from secondary electron and backscattered electron detectors for topography and additional material information, respectively).

Fig. S2. Antibacterial effect of NETs on live *S. aureus*, controls of IF microscopy and line plot analysis of naRNA and LL37

(A) Extracellular bactericidal activity of human PMN/NETs after infection with *S. aureus* and treatment with RNase A and DNase I during or after formation of PMA-induced NETs (n = 8, combined data, mean+SD, *p<0.05 according to one-way ANOVA). **(B)** Confocal microscopy of unstimulated or PMA-stimulated primary human PMNs (control to Fig. 2B) after 3 h, stained DNA (Hoechst 33342, white; n = 9, representative images; scale bar: 10 µm). **(C)** as in **B** but controls of Fig. 2D (n = 3). **(D)** as in **B** but controls of Fig. 2F (n = 3). **(E)** Confocal microscopy of primary human PMNs stimulated as indicated for 3 h and stained for naRNA (anti-rRNA Y10b, magenta), LL37 (anti-hLL37-DyLight550, yellow) and DNA (Hoechst 33342, white; n = 3, representative images, scale bar 10 µm). The line plot analysis of LL37, RNA and DNA staining was performed using ZenBlue3 software (n=2). Two different line plots from the same representative image are shown.

Fig. S3. Inhibition of PAD4 in human PMNs during NET formation assay and Unc93b1$^{-/-}$ BM-PMN stimulation with human NETs

(A) Confocal microscopy of stimulated primary human PMNs after 3 h and stained for DNA (Hoechst 33342, white) in the presence or absence of the PAD4-inhibitor Cl-amidine (200 µM, n = 3, representative images; scale bar 10 µm). **(B)** Confocal microscopy of unstimulated primary C57BL/6 WT or *Unc93b1*$^{-/-}$ murine BM-PMNs stimulated as indicated for 16 h as in **A** (n = 3 WT, n = 1 *Unc93b1*$^{-/-}$, representative images, scale bar: 10 µm).

Fig. S4. Immune responses of PBMCs, macrophages, and NK-cells to NETs and in vivo fluorescence imaging

(A) Triplicate IL-8 ELISA from WT, *TLR8*$^{-/-}$ and *TLR7*$^{-/-}$ THP-1 cells stimulated as indicated for 18 h, normalized to PMA+ionomycin control (n = 4, combined data, mean+SD, each dot represents one biological replicate, *p<0.05 according to one-way ANOVA). **(B-D)** Triplicate ELISA for TNF (**A**, n = 4), IL-6 (**B**, n = 3), and IL-8 (**C**, n = 3) from primary human PBMCs stimulated as indicated with/without CU-CPT9a for 24 h (combined data, mean+SD, each dot represents one biological replicate, *p<0.05

according to one-way ANOVA). **(E)** Triplicate IFN-γ ELISA from NK-92 MI cells stimulated as indicated for 24 h (n = 3, combined data, mean+SD, each dot represents one biological replicate, *p<0.05 according to one-way ANOVA).

Fig. S5. Graphical abstract

Supplemental movie S1: 3D reconstruction of NET DNA network decorated with naRNA

Confocal microscopy of primary human PMNs stimulated with PMA for 3 h, stained for naRNA (anti-rRNA Y10b, magenta) and DNA (Hoechst 33342, white; n = 3) and 3D analysis and animation were performed.

Supplemental movie S2: Digest of naRNA in PMA-induced NETs

Confocal live microscopy of RNase digestion of NETs obtained from primary human PMNs stimulated with PMA for 3 h, stained for naRNA (SYTO RNAselect, magenta) and DNA (Hoechst 33342, white; n = 3). RNase A was added, and live cell imaging was immediately started (n = 3, scale bar 20 µm).

Supplemental movie S3: DNase degrades not only DNA but also naRNA in NETs

Confocal live microscopy of DNase digestion of NETs obtained from primary human PMNs stimulated with PMA for 3 h, stained for naRNA (SYTO RNAselect, magenta) and DNA (Hoechst 33342, white; n = 3). DNase I was added, and live cell imaging was immediately started (n = 3, scale bar 20 µm).

References

Altincicek, B., S. Stotzel, M. Wygrecka, K. T. Preissner and A. Vilcinskas (2008). "Host-derived extracellular nucleic acids enhance innate immune responses, induce coagulation, and prolong survival upon infection in insects." J Immunol **181**(4): 2705-2712.

Balak, D. M., M. B. van Doorn, R. D. Arbeit, R. Rijneveld, E. Klaassen, T. Sullivan, J. Brevard, H. B. Thio, E. P. Prens, J. Burggraaf and R. Rissmann (2017). "IMO-8400, a toll-like receptor 7, 8, and 9 antagonist, demonstrates clinical activity in a phase 2a, randomized, placebo-controlled trial in patients with moderate-to-severe plaque psoriasis." Clin Immunol **174**: 63-72.

Bitschar, K., B. Sauer, J. Focken, H. Dehmer, S. Moos, M. Konnerth, N. A. Schilling, S. Grond, H. Kalbacher, F. C. Kurschus, F. Gotz, B. Krismer, A. Peschel and B. Schittek (2019). "Lugdunin amplifies innate immune responses in the skin in synergy with host- and microbiota-derived factors." Nat Commun **10**(1): 2730.

Bitschar, K., L. Staudenmaier, L. Klink, J. Focken, B. Sauer, B. Fehrenbacher, F. Herster, Z. Bittner, L. Bleul, M. Schaller, C. Wolz, A. N. R. Weber, A. Peschel and B. Schittek (2020). "Staphylococcus aureus Skin Colonization Is Enhanced by the Interaction of Neutrophil Extracellular Traps with Keratinocytes." J Invest Dermatol **140**(5): 1054-1065 e1054.

Boeltz, S., P. Amini, H. J. Anders, F. Andrade, R. Bilyy, S. Chatfield, I. Cichon, D. M. Clancy, J. Desai, T. Dumych, N. Dwivedi, R. A. Gordon, J. Hahn, A. Hidalgo, M. H. Hoffmann, M. J. Kaplan, J. S. Knight, E. Kolaczkowska, P. Kubes, M. Leppkes, A. A. Manfredi, S. J. Martin, C. Maueroder, N. Maugeri, I. Mitroulis, L. E. Munoz, D. Nakazawa, I. Neeli, V. Nizet, E. Pieterse, M. Z. Radic, C. Reinwald, K. Ritis, P. Rovere-Querini, M. Santocki, C. Schauer, G. Schett, M. J. Shlomchik, H. U. Simon, P. Skendros, D. Stojkov, P. Vandenabeele, T. V. Berghe, J. van der Vlag, L. Vitkov, M. von Kockritz-Blickwede, S.

Yousefi, A. Zarbock and M. Herrmann (2019). "To NET or not to NET:current opinions and state of the science regarding the formation of neutrophil extracellular traps." Cell Death Differ **26**(3): 395-408.
Brinkmann, V., U. Reichard, C. Goosmann, B. Fauler, Y. Uhlemann, D. S. Weiss, Y. Weinrauch and A. Zychlinsky (2004). "Neutrophil extracellular traps kill bacteria." Science **303**(5663): 1532-1535.
Chang, T.-H., Y. C. Gloria, M. J. Hellmann, C. L. Greve, D. L. Roy, T. Roger, L. Kasper, B. Hube, S. Pusch, N. Gow, M. Sørlie, A. Tøndervik, B. M. Moerschbacher and A. N. R. Weber (2022). "Transkingdom mechanism of MAMP generation by chitotriosidase (CHIT1) feeds oligomeric chitin from fungal pathogens and allergens into TLR2-mediated innate immune sensing." bioRxiv: 2022.2002.2017.479713.
Coch, C., B. Hommertgen, T. Zillinger, J. Dassler-Plenker, B. Putschli, M. Nastaly, B. M. Kummerer, J. F. Scheunemann, B. Schumak, S. Specht, M. Schlee, W. Barchet, A. Hoerauf, E. Bartok and G. Hartmann (2019). "Human TLR8 Senses RNA From Plasmodium falciparum-Infected Red Blood Cells Which Is Uniquely Required for the IFN-gamma Response in NK Cells." Front Immunol **10**: 371.
Colak, E., A. Leslie, K. Zausmer, E. Khatamzas, A. V. Kubarenko, T. Pichulik, S. N. Klimosch, A. Mayer, O. Siggs, A. Hector, R. Fischer, B. Klesser, A. Rautanen, M. Frank, A. V. Hill, B. Manoury, B. Beutler, D. Hartl, A. Simmons and A. N. Weber (2014). "RNA and imidazoquinolines are sensed by distinct TLR7/8 ectodomain sites resulting in functionally disparate signaling events." J Immunol **192**(12): 5963-5973.
Dickson, M. A., W. C. Hahn, Y. Ino, V. Ronfard, J. Y. Wu, R. A. Weinberg, D. N. Louis, F. P. Li and J. G. Rheinwald (2000). "Human keratinocytes that express hTERT and also bypass a p16(INK4a)-enforced mechanism that limits life span become immortal yet retain normal growth and differentiation characteristics." Mol Cell Biol **20**(4): 1436-1447.
Doster, R. S., L. M. Rogers, J. A. Gaddy and D. M. Aronoff (2018). "Macrophage Extracellular Traps: A Scoping Review." J Innate Immun **10**(1): 3-13.
Eigenbrod, T. and A. H. Dalpke (2015). "Bacterial RNA: An Underestimated Stimulus for Innate Immune Responses." J Immunol **195**(2): 411-418.
Faust, N., F. Varas, L. M. Kelly, S. Heck and T. Graf (2000). "Insertion of enhanced green fluorescent protein into the lysozyme gene creates mice with green fluorescent granulocytes and macrophages." Blood **96**(2): 719-726.
Fruh, A., K. Tielking, F. Schoknecht, S. Liu, U. C. Schneider, S. Fischer, P. Vajkoczy and R. Xu (2021). "RNase A Inhibits Formation of Neutrophil Extracellular Traps in Subarachnoid Hemorrhage." Front Physiol **12**: 724611.
Ganguly, D., G. Chamilos, R. Lande, J. Gregorio, S. Meller, V. Facchinetti, B. Homey, F. J. Barrat, T. Zal and M. Gilliet (2009). "Self-RNA-antimicrobial peptide complexes activate human dendritic cells through TLR7 and TLR8." J Exp Med **206**(9): 1983-1994.
Gilliet, M., C. Conrad, M. Geiges, A. Cozzio, W. Thurlimann, G. Burg, F. O. Nestle and R. Dummer (2004). "Psoriasis triggered by toll-like receptor 7 agonist imiquimod in the presence of dermal plasmacytoid dendritic cell precursors." Arch Dermatol **140**(12): 1490-1495.
Heil, F., H. Hemmi, H. Hochrein, F. Ampenberger, C. Kirschning, S. Akira, G. Lipford, H. Wagner and S. Bauer (2004). "Species-specific recognition of single-stranded RNA via toll-like receptor 7 and 8." Science **303**(5663): 1526-1529.
Herster, F., Z. Bittner, N. K. Archer, S. Dickhofer, D. Eisel, T. Eigenbrod, T. Knorpp, N. Schneiderhan-Marra, M. W. Loffler, H. Kalbacher, T. Vierbuchen, H. Heine, L. S. Miller, D. Hartl, L. Freund, K. Schakel, M. Heister, K. Ghoreschi and A. N. R. Weber (2020). "Neutrophil extracellular trap-associated RNA and LL37 enable self-amplifying inflammation in psoriasis." Nat Commun **11**(1): 105.
Ishii, N., K. Funami, M. Tatematsu, T. Seya and M. Matsumoto (2014). "Endosomal localization of TLR8 confers distinctive proteolytic processing on human myeloid cells." J Immunol **193**(10): 5118-5128.
Jiang, W., F. G. Zhu, L. Bhagat, D. Yu, J. X. Tang, E. R. Kandimalla, N. La Monica and S. Agrawal (2013). "A Toll-like receptor 7, 8, and 9 antagonist inhibits Th1 and Th17 responses and inflammasome activation in a model of IL-23-induced psoriasis." J Invest Dermatol **133**(7): 1777-1784.
Knight, J. S., W. Luo, A. A. O'Dell, S. Yalavarthi, W. Zhao, V. Subramanian, C. Guo, R. C. Grenn, P. R. Thompson, D. T. Eitzman and M. J. Kaplan (2014). "Peptidylarginine deiminase inhibition reduces

vascular damage and modulates innate immune responses in murine models of atherosclerosis." Circ Res **114**(6): 947-956.
Kruger, P., M. Saffarzadeh, A. N. Weber, N. Rieber, M. Radsak, H. von Bernuth, C. Benarafa, D. Roos, J. Skokowa and D. Hartl (2015). "Neutrophils: Between host defence, immune modulation, and tissue injury." PLoS Pathog **11**(3): e1004651.
Kulkarni, N. N., A. M. O'Neill, T. Dokoshi, E. W. C. Luo, G. C. L. Wong and R. L. Gallo (2021). "Sequence determinants in the cathelicidin LL-37 that promote inflammation via presentation of RNA to scavenger receptors." J Biol Chem **297**(1): 100828.
Lande, R., J. Gregorio, V. Facchinetti, B. Chatterjee, Y. H. Wang, B. Homey, W. Cao, Y. H. Wang, B. Su, F. O. Nestle, T. Zal, I. Mellman, J. M. Schroder, Y. J. Liu and M. Gilliet (2007). "Plasmacytoid dendritic cells sense self-DNA coupled with antimicrobial peptide." Nature **449**(7162): 564-569.
Lerner, E. A., M. R. Lerner, C. A. Janeway, Jr. and J. A. Steitz (1981). "Monoclonal antibodies to nucleic acid-containing cellular constituents: probes for molecular biology and autoimmune disease." Proc Natl Acad Sci U S A **78**(5): 2737-2741.
Li, M., C. Lin, H. Deng, J. Strnad, L. Bernabei, D. T. Vogl, J. J. Burke and Y. Nefedova (2020). "A Novel Peptidylarginine Deiminase 4 (PAD4) Inhibitor BMS-P5 Blocks Formation of Neutrophil Extracellular Traps and Delays Progression of Multiple Myeloma." Mol Cancer Ther **19**(7): 1530-1538.
Li, X. D. and Z. J. Chen (2012). "Sequence specific detection of bacterial 23S ribosomal RNA by TLR13." Elife **1**: e00102.
Mahdavian Delavary, B., W. M. van der Veer, M. van Egmond, F. B. Niessen and R. H. Beelen (2011). "Macrophages in skin injury and repair." Immunobiology **216**(7): 753-762.
Mollerherm, H., M. von Kockritz-Blickwede and K. Branitzki-Heinemann (2016). "Antimicrobial Activity of Mast Cells: Role and Relevance of Extracellular DNA Traps." Front Immunol **7**: 265.
Munzer, P., R. Negro, S. Fukui, L. di Meglio, K. Aymonnier, L. Chu, D. Cherpokova, S. Gutch, N. Sorvillo, L. Shi, V. G. Magupalli, A. N. R. Weber, R. E. Scharf, C. M. Waterman, H. Wu and D. D. Wagner (2021). "NLRP3 Inflammasome Assembly in Neutrophils Is Supported by PAD4 and Promotes NETosis Under Sterile Conditions." Front Immunol **12**: 683803.
Neumann, E., R. Hasseli, U. Lange and U. Muller-Ladner (2018). "The Role of Extracellular Nucleic Acids in Rheumatoid Arthritis." Curr Pharm Biotechnol **19**(15): 1182-1188.
Preissner, K. T., S. Fischer and E. Deindl (2020). "Extracellular RNA as a Versatile DAMP and Alarm Signal That Influences Leukocyte Recruitment in Inflammation and Infection." Front Cell Dev Biol **8**: 619221.
Presolski, S. I., V. P. Hong and M. G. Finn (2011). "Copper-Catalyzed Azide-Alkyne Click Chemistry for Bioconjugation." Curr Protoc Chem Biol **3**(4): 153-162.
Sacre, S., A. Lo, B. Gregory, M. Stephens, G. Chamberlain, P. Stott and F. Brennan (2016). "Oligodeoxynucleotide inhibition of Toll-like receptors 3, 7, 8, and 9 suppresses cytokine production in a human rheumatoid arthritis model." Eur J Immunol **46**(3): 772-781.
Sacre, S. M., A. Lo, B. Gregory, R. E. Simmonds, L. Williams, M. Feldmann, F. M. Brennan and B. M. Foxwell (2008). "Inhibitors of TLR8 reduce TNF production from human rheumatoid synovial membrane cultures." J Immunol **181**(11): 8002-8009.
Schmidt, B., E. Engel, T. Carstensen, S. Weickmann, M. John, C. Witt and M. Fleischhacker (2005). "Quantification of free RNA in serum and bronchial lavage: a new diagnostic tool in lung cancer detection?" Lung Cancer **48**(1): 145-147.
Simsekyilmaz, S., H. A. Cabrera-Fuentes, S. Meiler, S. Kostin, Y. Baumer, E. A. Liehn, C. Weber, W. A. Boisvert, K. T. Preissner and A. Zernecke (2014). "Role of extracellular RNA in atherosclerotic plaque formation in mice." Circulation **129**(5): 598-606.
Sioud, M. (2020). "RNA Interference and CRISPR Technologies Technical Advances and New Therapeutic Opportunities Preface." Rna Interference and Crispr Technologies: Technical Advances and New Therapeutic Opportunities **2115**: V-Vii.
Song, W., J. Ye, N. Pan, C. Tan and M. Herrmann (2020). "Neutrophil Extracellular Traps Tied to Rheumatoid Arthritis: Points to Ponder." Front Immunol **11**: 578129.

Sorensen, O., K. Arnljots, J. B. Cowland, D. F. Bainton and N. Borregaard (1997). "The human antibacterial cathelicidin, hCAP-18, is synthesized in myelocytes and metamyelocytes and localized to specific granules in neutrophils." Blood **90**(7): 2796-2803.
Tabeta, K., K. Hoebe, E. M. Janssen, X. Du, P. Georgel, K. Crozat, S. Mudd, N. Mann, S. Sovath, J. Goode, L. Shamel, A. A. Herskovits, D. A. Portnoy, M. Cooke, L. M. Tarantino, T. Wiltshire, B. E. Steinberg, S. Grinstein and B. Beutler (2006). "The Unc93b1 mutation 3d disrupts exogenous antigen presentation and signaling via Toll-like receptors 3, 7 and 9." Nat Immunol **7**(2): 156-164.
Vierbuchen, T., C. Bang, H. Rosigkeit, R. A. Schmitz and H. Heine (2017). "The Human-Associated Archaeon Methanosphaera stadtmanae Is Recognized through Its RNA and Induces TLR8-Dependent NLRP3 Inflammasome Activation." Front Immunol **8**: 1535.
Vlach, J., A. T. Bender, M. Przetak, A. Pereira, A. Deshpande, T. L. Johnson, S. Reissig, E. Tzvetkov, D. Musil, N. T. Morse, P. Haselmayer, S. C. Zimmerli, S. L. Okitsu, R. L. Walsky and B. Sherer (2021). "Discovery of M5049: A Novel Selective Toll-Like Receptor 7/8 Inhibitor for Treatment of Autoimmunity." J Pharmacol Exp Ther **376**(3): 397-409.
Warnatsch, A., M. Ioannou, Q. Wang and V. Papayannopoulos (2015). "Inflammation. Neutrophil extracellular traps license macrophages for cytokine production in atherosclerosis." Science **349**(6245): 316-320.
Zack, G. W., W. E. Rogers and S. A. Latt (1977). "Automatic-Measurement of Sister Chromatid Exchange Frequency." Journal of Histochemistry & Cytochemistry **25**(7): 741-753.
Zernecke, A. and K. T. Preissner (2016). "Extracellular Ribonucleic Acids (RNA) Enter the Stage in Cardiovascular Disease." Circ Res **118**(3): 469-479.
Zhang, S., Z. Hu, H. Tanji, S. Jiang, N. Das, J. Li, K. Sakaniwa, J. Jin, Y. Bian, U. Ohto, T. Shimizu and H. Yin (2018). "Small-molecule inhibition of TLR8 through stabilization of its resting state." Nat Chem Biol **14**(1): 58-64.

Additional information

Author contributions: according to Credit guidelines:

	FB	CGL	CY	SC	YW	MN	JF	JS	PE	MD	KH	BS	MWL	YS	NKA	AM
Conceptualization	x															
Data curation																
Formal analysis	x	x	x	x		x	x	x	x		x				x	
Funding acquisition												x				
Investigation	x	x	x	x		x	x	x	x	x	X					
Methodology											X			x		
Project administration					x								X			
Resources													X			
Software																
Supervision	X											x		x	x	
Validation	X														x	
Visualization	x	x	x								X					
Writing: original draft	x															
Writing: review and editing	x	x	x	x	x	x	x	x	x	x	x	x	x	x	x	

Conflict of interest statement

NKA has received previous grant support from Pfizer and Boehringer Ingelheim and was a paid consultant for Janssen Pharmaceuticals. All other authors declare no competing interests. S.D.G.

Acknowledgments

We gratefully acknowledge Jim Rheinwald, Holger Heine, Austin Chang, Thomas Zillinger for the provision of reagents, respectively, and Jon Kagan and Libera Lo Presti for helpful scientific and editorial comments. We thank all voluntary healthy donors of biomaterials for participating in the study. The study was supported by the Deutsche Forschungsgemeinschaft (German Research Foundation, DFG) grants CRC TR156 “The skin as an immune sensor and effector organ – Orchestrating local and systemic immunity” (to FB, CG, JF, JS, BS and ANRW), NIH grants R01AI146177, R01AR073665, and R01AR069502 (to NKA). NKA. has received previous grant support from Pfizer and Boehringer Ingelheim and was a paid consultant for Janssen Pharmaceuticals. Infrastructural funding was provided by the University of Tübingen, the University Hospital Tübingen and the DFG Clusters of Excellence "iFIT – Image-Guided and Functionally Instructed Tumor Therapies" (EXC 2180, to AW, PE, BS and MWL), “CMFI – Controlling Microbes to Fight Infection (EXC 2124 to AW and BS). Gefördert durch die Deutsche Forschungsgemeinschaft (DFG) im Rahmen der Exzellenzstrategie des Bundes und der Länder - EXC 2180 and EXC 2124. The authors declare no competing financial interests.

Abbreviations

AF – Alexa Fluor; bRNA – bacterial ribonucleic acid; DAMP – damage-associated molecular pattern; 5-EU – 5-Ethynyluridine; FACS – Fluorescence Activated Cell Sorting; fRNA – fungal ribonucleic acid; HEK – Human embryonic kidney; HMGB-1 – High-Mobility-Group-Protein B1; HSC – hematopoietic stem cell; IFN – Interferon; IL – Interleukin; KO – knockout; MCET – Mast cell extracellular trap; MET – Macrophage extracellular trap; MPO – Myeloperoxidase; naRNA – Neutrophil extracellular trap-associated RNA; NET – Neutrophil extracellular trap; NK – natural killer; PAD4 - Peptidyl arginine deiminase 4; PBMC - Peripheral Blood Mononuclear Cell; PKC- Protein kinase C; PMN – Polymorphonuclear leukocytes; RT – room temperature; SEM – scanning electron microscopy; TLR – Toll-like receptor; TNF – Tumor necrosis factor

Materials and Methods

Reagents

PMA (tlrl-pma), Nigericin (tlrl-nig), LL37 (tlrl-l37), as well as the PRR ligands LPS (tlrl-peklps), R848 (tlrl-r848), TL8 (tlrl-tl8506), and the TLR8-inhibitor CU-CPT9a (inh-cc9a) were from Invivogen, Ionomycin was acquired from Sigma (I0634-1MG). RNase inhibitor (N2615) was from Promega, RNase A (EN0531), DNase I (EN0521) and DNase inhibitor (EN0521) were from Thermo Fisher. The PAD4-inhibitor Cl-amidine (506282) was from Merck Millipore. DOTAP (L787.2) was from Roth (see Supplementary Table S1) and ssRNA40 was from Eurogentec (see Supplementary Table S2). Bacterial RNA isolated from *S. aureus* was prepared as described (Herster, Bittner et al. 2020). Fungal RNA from *C. albicans* strain SC5314 was isolated as described below, as well as naRNA isolated from PMA NETs. For complex formation to stimulate cells in a volume of 500 µL, 5.8 µM ssRNA40 (~ 34.4 µg/mL), fungal RNA (125 ng/mL), bacterial RNA (10 µg/mL) or PMA NET derived naRNA (~ 600 ng/mL) was mixed with 10 µg LL37 and left for 1 h at room temperature (RT). For a smaller volume of cells, complexes were used in the according fractional amount. For RNA-only or LL37-only controls, the same amounts and volumes were used replacing one of the components with sterile, endotoxin-free H_2O. For complex formation with DOTAP, the according RNA or CpG was incubated with the transfection reagent for 10 min at RT prior to stimulation of the cells. NET content for stimulation was prepared as described below. Antibodies used for fluorescence microscopy, as well as click chemistry reagents are listed in Supplementary Tables S3 and S4. Constructs used for transfection of HEK293T cells are listed in Supplementary Table S5.

Preparation of fungal RNA from *C. albicans*

C. albicans SC5314 (kindly cultured and prepared by Tzu-Hsuan Chang, Tübingen) was plated in a slant tube containing YPD agar and grown overnight at 30 °C as described in (Chang, Gloria et al. 2022). One colony was picked from the slant tube and resuspended in 500 µL YPD medium, centrifuged at 10,000 rpm for 1 min and washed with phosphate-buffered saline (PBS). Afterwards, the pellet was resuspended in 200 µL RLT buffer (derived from RNeasy Mini Kit, Qiagen, #74106) and transferred into a 2 mL tube containing 0.5 mm diameter ceramic beads. The tube was filled up to 1 mL with RLT buffer and the fungi were subsequently homogenized by using a microtube homogenizer (BeadBug™, Merck) with an interval of seven times 2 min shaking at 2800 rpm and 1 min cooling break on ice. The supernatant was transferred into a new tube containing 1 mL 75% ethanol (VWR, 20821.330). The further RNA isolation was performed according to the manufacturer's instructions using the Qiagen RNeasy Mini Kit for purification of Total RNA from Animal Tissues (RNeasy Mini Kit, Qiagen, 74106). The RNA was eluted in 30 µL RNase DNase-free H_2O and the concentration was determined with a Nanodrop Spectrophotometer.

Mice

Unc93b1$^{3d/3d}$ (Tabeta, Hoebe et al. 2006), *Tlr13*$^{-/-}$ (Li and Chen 2012) (both kindly provided by Tatjana Eigenbrod, Heidelberg and on C57BL/6 background) and WT C57BL/6 mice between 8 and 20 weeks of age were used in accordance with local institutional guidelines on animal experiments, regular hygiene monitoring, and specific locally approved protocols compliant with the German regulations of the Gesellschaft für Versuchstierkunde/Society for Laboratory Animal Science (GV-SOLAS) and the European Health Law of the Federation of Laboratory Animal Science Associations (FELASA) for sacrificing and *in vivo* work. *Unc93b1*$^{3d/3d}$, *Tlr13*$^{-/-}$ and WT C57BL/6 control mice were housed in controlled specific-pathogen-free animal facilities at the Interfaculty Institute of Cell Biology, Tübingen. Local federal authority for the approval of experimental protocols was the Regierungspräsidium Tübingen. LysM$^{EGFP/+}$ (Faust, Varas et al. 2000), *Tlr13*$^{-/-}$ mice (Li and Chen 2012) (kindly provided by James Chen, Houston and David Nemazee, La Jolla) and WT (all on a C57BL/6 background) mouse strains were also bred and maintained under the specific pathogen-free conditions, with air isolated cages at an American Association for the Accreditation of Laboratory Animal Care (AAALAC)-accredited

animal facility at Johns Hopkins University and handled according to procedures described in the Guide for the Care and Use of Laboratory Animals as well as Johns Hopkins University's policies and procedures as set forth in the Johns Hopkins University Animal Care and Use Training Manual, and all animal experiments were approved by the Johns Hopkins University Animal Care and Use Committee (MO21M378). Gender-and age-matched 6-8 week old mice were used for each experiment.

Isolation and stimulation of primary bone-marrow-derived polymorphonuclear neutrophils (BM-PMNs)

Bone-marrow (BM)-PMNs were isolated from the bone marrow as described (Herster, Bittner et al. 2020). In brief, bones were isolated from the respective mice and the bone marrow was flushed out. Afterwards, neutrophils were isolated using magnetic separation (mouse Neutrophil isolation kit, Miltenyi Biotec, 130-097-658) following the manufacturer's instructions. In total, 1×10^5 cells/well PMNs were seeded in a 24-well plate, and stimulation was carried out with PMA (600 nM), ssRNA+LL37 complex (as previously described), nigericin (50 µM), live *C. albicans* (MOI1) or human NET content (mock control and PMA NETs, 1:50 dilution) for 16 h at 37°C and 5% CO2. Subsequently, cells were stained for immunofluorescence.

Study participants and human blood or tissue sample acquisition

All healthy donors included in this study provided their written informed consent before participation. Approval for use of biomaterials was obtained for this project by the local ethics committee of the Medical Faculty Tübingen in accordance with the principles laid down in the Declaration of Helsinki as well as applicable laws and regulations.

Primary human neutrophil isolation and stimulation

Neutrophils of healthy human donors were isolated as described (Herster, Bittner et al. 2020). In brief, EDTA-anticoagulated whole blood was diluted in PBS (Thermo Fisher, 14190-169), loaded on Ficoll (1.077 g/mL, Sigma, 10771) and centrifuged for 25 min at 509 x g at RT without brake. Afterwards, all layers except the erythrocyte-granulocyte layer were discarded and erythrocyte lysis was performed twice (for 20 and for 10 min) using 1x ammonium chloride erythrocyte lysis buffer (see Supplementary Table S6) at 4 °C on roller shaker. The remaining cells were resuspended in culture medium (RPMI culture medium (Sigma-Aldrich, R8758) + 10% FBS (heat-inactivated, sterile filtered, Th. Geyer, 11682258)) to a concentration of 1.6 x 10^6 cells/mL. 500 µL of cells were seeded in a 24-well plate for immunofluorescence microscopy or 8 mL of 5 x 10^6 cells/mL in 10 cm uncoated dishes for NET preparation and naRNA isolation/isolation of whole PMN RNA. After seeding, the cells were rested for 30 min at 37°C and 5% CO_2, followed by 3 h stimulation with PMA (600 nM), nigericin (50 µM), live *C. albicans* (MOI2), RNA+LL37 complexes (as previously described) or NET content at indicated dilutions for IF or 4 h stimulation with PMA (600 nM) for NET preparation. Where indicated, the cells were incubated with 100 nM TLR8-inhibitor CU-CPT9a or 200 µM PAD4-inhibitor Cl-amidine 30 min before stimulation and not replaced during incubation with the respective stimuli.

Primary peripheral blood mononuclear cells (PBMC) isolation and stimulation

PBMCs were isolated from whole blood or buffy coats as described (Herster, Bittner et al. 2020). In brief, EDTA-anticoagulated blood was diluted in PBS and density gradient separation was performed as described above. The PBMC layer was then carefully transferred into another reaction tube and diluted in PBS (1:1). The cell suspension was spun down at 645 × g for 8 min and the cells were washed two more times in PBS and resuspended in culture medium (RPMI + 10% FBS (heat inactivated) +1% L-glutamine) at a density of 1 x 10^6 cells/mL. Afterwards, 200 µL of PBMCs were seeded in a 96-well plate and stimulated with LPS (100 ng/mL), R848 (5 µg/mL), TL8 (100 ng/mL), ssRNA (1.6 µg/mL) + DOTAP (50 µg/mL), ssRNA+LL37 complex (as described above), and respective NET content (1:20 dilution) for 24 h at 37°C and 5% CO_2. Where indicated, the TLR8 inhibitor CU-CPT9a was added to the cells at a concentration of 1 µM 2h before stimulation and was not removed for the incubation of the cells with the respective stimuli. After the stimulation, the plate was centrifuged for 5 min at 1500 rpm and the supernatant was collected and stored at -80 °C until the ELISA was performed.

Preparation of NETs and isolation of naRNA/whole PMN RNA

NETs were prepared by 600 nM PMA treatment for 4 h at 37°C and 5% CO_2, or cells were left untreated during the incubation as the mock control. After incubation, the neutrophils were gently washed three times with PBS to get rid of PMA as the stimulus for NET formation, any cytokines released by the cells and unstimulated PMNs, as those do not adhere to the uncoated petri dish used here. In some conditions (as indicated) during the NET preparation process and for storage, naRNA was protected by addition of 10 U/µL RNase inhibitor (= Mock or PMA NETs + RNase Inhibitor). For digest of NETs with the respective enzymes, the NET content was incubated for 20 min at 37 °C with RNase A (Thermo Fisher, EN0531; 100 µg/mL, EDTA for DNase inhibition added) or DNase I (Thermo Fisher, EN0521) for 60 min at 37 °C (1 U/10 µL, RNase inhibitor for RNase inhibition added). For isolation of naRNA, RNase inhibitor was added to the PMNs during NET formation. After the above described washing process, PMA or mock NETs were resuspended in 300 µL of ML buffer and RNA isolation was performed according to the manufacturer's instructions (NucleoSpin miRNA isolation kit, Macherey-Nagel, 740971.50). The RNA was eluted in 50 µL RNase/DNase/endotoxin-free H2O and the concentration was determined with a Nanodrop Spectrophotometer. For isolation of whole PMN RNA, untreated PMNs were directly lysed, and the RNA was isolated from the cells according to the manufacturer's instructions.

Preparation of human primary stem cell-derived PMNs

Stem cells derived from human healthy donors were prepared and differentiated as described (Sioud 2020). In brief, bone marrow was diluted in PBS, carefully layered on Ficoll-Paque medium (density: 1.077 g/mL) and centrifuged at 500 x g for 25 min at RT without brakes. The interphase layer containing the mononuclear cell fraction was transferred to a new tube and washed twice with 30 mL ice-cold PBS by centrifugation at 300 x g for 8 min at 8 °C. Further, the cells were resuspended, counted, and isolated using Human CD34 MicroBead Kit (Miltenyi) for magnetic beads-based isolation of $CD34^+$ cells from BMMNCs . Afterwards, the number of $CD34^+$ HPSCs was determined and cultured in $CD34^+$ culture medium (Stemline II Hematopoietic Stem Cell Expansion medium supplemented with 10% FCS, 1% L-glutamine, 1% penicillin/streptomycin, and a human recombinant cytokine cocktail consisting of 20 ng/mL IL-3, 20 ng/ mL IL-6, 20 ng/mL TPO, 50 ng/mL SCF, and 50 ng/mL FLT-3L) at a density of 2 x 10^5/mL at 37 °C and 5% CO_2. The medium was replaced every second day and the cells were cultured for 14 days. During the differentiation process, the cells were treated with 100 µM 5-ethynyl uridine for 14 days for subsequent click chemistry labeling of endogenous RNA or were left untreated as negative controls. To verify differentiation, cell morphology was assessed using Cytospin assay. In brief, the Cytoclip™ slide clips were loaded by fitting the filter card, the sample chamber, and the glass slide. An assemble Cytoclip™ slide clip was then placed in the slide clip support plate of the cytospin centrifuge. 2 x 10^4 cells from liquid culture differentiation were pipetted into Cytofunnel™ and centrifuged for 3 min at 200 x g. The cytospin slides were stained for 5 min in May-Grünwald stain, rinsed shortly with ddH2O, and then stained for 10 min in Wright-Giemsa stain. Afterwards, the slides were rinsed shortly with ddH2O and cell morphology was determined using a microscope. To further verify differentiation, flow cytometric analysis was performed using antibodies specific for the following hematopoietic/myeloid markers: CD45 (leukocyte marker), CD34 (HSPC marker), CD33 (promyelocyte marker), CD11b (myeloid cell marker), CD14 (monocyte marker), and CD15 and CD16 (neutrophil markers). Neutrophil percentage was determined by gating on neutrophils as follows: $CD45^+CD11b^+CD15^+$, or $CD45^+CD11b^+CD16^+$, or $CD45^+CD15^+CD16^+$ cells

BlaER1 cell culture, transdifferentiation and stimulation

BlaER1 cells (WT, *Unc93b*$^{-/-}$ and *Tlr8*$^{-/-}$), a kind gift of Holger Heine, Borstel, Germany (Vierbuchen, Bang et al. 2017), were cultured, transdifferentiated, and stimulated for 18 h with the respective stimuli as described (Herster, Bittner et al. 2020). In brief, 1x10^6 cells/well were seeded in a 6-well plate and differentiated with 10 ng/mL hIL-3, 10 ng/mL hMCSF and 150 nM β-estradiol in complete RPMI-1640 (PANBiotech, P04-18525) for 7 days. Afterwards 5 x 10^4 differentiated cells were reseeded in a 96-well plate, followed by 1 h resting. Cells were treated with the respective stimuli (LPS at 0.1 µg/mL, R848 at

5 µg/mL, the TLR8 agonist TL8 at 100 ng/mL or ssRNA+LL37 complex as described above) and Mock or PMA NETs with or without RNase inhibitor) in complete medium in a total volume of 125 µL/well for 18 h. After stimulation, the cells were centrifuged for 5 min at 1200 rpm, the supernatant was transferred into a new plate and stored at -80°C until the ELISA was performed.

THP-1 cell culture, differentiation and stimulation

THP-1 cells (THP-1 cells were a kind gift from Thomas Zillinger, Bonn, Germany (Coch, Hommertgen et al. 2019), were cultured in complete RPMI-1640 (Sigma, R8758-24X500ML) medium. For differentiation into macrophage-like cells, 5 x 10^4 cells/well were seeded in a 96-well plate, treated with 300 ng/mL PMA and incubated for 16 h at 37°C and 5% CO_2. The next day, the cells were washed three times with PBS and fresh medium was added, followed by 48 h of resting. Subsequently, the medium was removed, exchanged by medium containing 200 U/mL IFN-γ (Sigma, I-3265), and the cells were incubated for 6 h. After repeated washing and medium exchange, cells were treated with the respective stimuli (PMA (25 µg/mL) + Ionomycin (0.375 µg/mL), LPS (0.1 µg/mL), R848 (5 µg/mL), TL8 (40 ng/mL), ssRNA+LL37 complex (as described above), Mock NETs + RNase inhibitor (1:50 dilution), PMA NETs (1:50 dilution) and PMA NETs + RNase inhibitor (1:50 dilution)) in complete medium in a total volume of 125 µL/well for 18 h. After stimulation, the cells were centrifuged for 5 min at 1200 rpm, the supernatant was transferred into a new plate and stored at -80°C until the ELISA was performed.

N/TERT-1 keratinocyte cell culture and stimulation

N/TERT-1 cells (a kind gift from Prof. James Rheinwald (Dickson, Hahn et al. 2000)) were cultured for less than ten passages in complete CnT-07 medium (CELLnTEC, CnT-07). Two days prior to stimulation, a total amount of 2 x 10^4 cells/well were seeded in a 96-well plate and incubated at 37°C and 5% CO_2. The medium was renewed, and the cells were stimulated in a total volume of 125 µL/well of the respective stimuli diluted in medium (PMA (25 µg/mL) + Ionomycin (0.375 µg/mL), TL8 (200 ng/mL), ssRNA+LL37 complex (as previously described), as well as Mock and PMA NETs with and without RNase inhibitor at indicated dilutions). After 24 h stimulation, the cells were centrifuged at 1200 rpm for 5 min and the supernatant was stored in a new plate at -80°C until further usage.

Primary normal human epidermal keratinocyte (NHEK) cell culture and stimulation

NHEK cells (Normal Human Epidermal Keratinocytes (NHEK) single juvenile donor, proliferating, PromoCell, C-12002) were grown and stimulated in Keratinocyte Growth Medium 2 (PromoCell, C-20111). Two days prior to stimulation, a total amount of 2 x 10^4 cells/well were seeded in a 96-well plate and incubated at 37°C and 5% CO_2. For stimulation, the medium was renewed with basal medium (PromoCell, C-20211) containing 1.7 mM $CaCl_2$ (Roth, CN93.1) and stimuli were added and diluted in medium in a final volume of 125 µL (R848 (20 µg/mL), TL8 (200 ng/mL), ssRNA+LL37 complex, as well as Mock NETs + RNase inhibitor (1:25 dilution) and PMA NETs with and without RNase inhibitor (1:25 dilution). After 24 h stimulation, the cells were centrifuged at 1200 rpm for 5 min and the supernatant was stored in a new plate at -80°C until further usage.

Preparation of 3D human skin equivalent

The 3D human skin equivalent was prepared as described (Bitschar, Staudenmaier et al. 2020). Briefly, primary fibroblasts were seeded on collagen and incubated in FF medium for five days. Subsequently, primary keratinocytes were added to the wells and airlifting was performed on day 12. On day 22, the 3D skin model was stimulated with NET content (25 µL/well for one 3D construct grown in a 12-well chamber) or respective water control for 24 h. Afterwards, supernatant was harvested for ELISA, RNA was isolated for qPCR analysis and H&E staining was performed.

NK-92 MI cell culture and stimulation

NK-92 MI cells (kindly provided by Melanie Märklin, University Hospital Tübingen) were cultured in IMDM-Medium (Lonza, 12-722F). For stimulation, a total amount of 1 x 10^5 cells/well were seeded in a volume of 200 µL and rested for 2 h at 37°C and 5% CO_2. The cells were stimulated with LPS (100

ng/mL), CpG (2.5 µM) + DOTAP (25 µg/mL), R848 (5 µg/mL), TL8 (100 ng/mL), ssRNA (1.6 µg/mL) + DOTAP (50 µg/mL), ssRNA+LL37 complex (as described above), or NET content (1:100 dilution) for 24 h and afterwards centrifuged for 5 min at 1500 rpm. Subsequently, the supernatant was transferred into a new plate and stored at -80°C until further usage.

Flow cytometry

After PMN isolation, the purity and activation status of the cells was determined by flow cytometry as described (Herster, Bittner et al. 2020). In brief, 200 µL of cells were transferred into a 96-well plate (U-bottom) and centrifuged for 5 min at 448 x g. Afterwards, blocking was performed using pooled human serum diluted 1:10 in PBS for 15 min at 4 °C. After washing, the samples were stained for 20 min at RT in the dark and fixed (4% PFA in PBS) after repeated washing for 10 min at RT in the dark. After an additional washing step, the cell pellets were resuspended in 300 µL PBS and measurements were performed on a FACS Canto II (BD Bioscience, Diva software). Analysis was performed using FlowJo V10 analysis software.

RNA sequencing analysis of naRNA

Isolated naRNA was analyzed for quality control using the Agilent 4200 TapeStation system. Subsequently, the RNA was sequenced according to NEBNext® Ultra™ II Directional RNA Library Prep Kit for Illumina®using the protocol for use with rRNA Depleted FFPE RNA. The data was quantified using Salmon Version1.5.0 and tximport was used to obtain the transcript-level quantification. For transcript classification, GENECODE annotation was performed.

Fluorescence microscopy of fixed human or murine primary neutrophils

500 µL of 1.6 x 10^6 cells/mL of human blood PMNs, and 2 x 10^6 cells/mL murine BM-PMNs were seeded in a 24-well plate containing poly-L-lysine-coated glass coverslips (Electron Microscopy Sciences, 72292-04) and rested for 30 min before stimulation at 37°C and 5% CO_2 with the according stimuli (as described above) for 3 h (human) or 16 h (murine), respectively, as adapted from Brinkmann *et al*., 2004 (Brinkmann, Reichard et al. 2004). After stimulation, the cells were carefully washed with PBS and fixed with fixation buffer (Biolegend, 420801) for 10 min at RT in the dark. Afterwards, the cells were blocked with PBS containing 0.1 % heat-inactivated diethylpyrocarbonate (DEPC) (Roth, K028.2), 10 % chicken serum (Normal Chicken Serum Blocking Solution S-3000, Biozol/Vectorlabs, VEC-S-3000-20), 0.1 % saponin (Applichem, A4518.0100), as well as 10 U/µL RNase inhibitor for 2 h at RT. The primary antibodies (rRNA Y10b, hLL37, see Supplementary Table S3) were diluted 1:50 in blocking buffer and subsequently incubated for 2 h at RT. Afterwards, the cells were washed three times with PBS containing 0.1 % heat-inactivated DEPC and incubated with the secondary antibodies (see Supplementary Table S3) in a 1:500 dilution in blocking buffer for 1 h. After repeated washing, the cells were incubated with Hoechst 33342 (Thermo Fisher; 1 µg/mL) for 5 min to stain nuclear DNA. Secondary antibodies alone did not yield any significant staining under identical staining and acquisition conditions. The coverslips were mounted (ProLong™ Diamond Antifade Mountant, Thermo Fisher, P36961) on glass slides and left to dry overnight at RT in the dark. Subsequently, the samples were stored at 4 °C before microscopy using a Zeiss LSM800 Confocal microscope (40x or 63x magnification with Z-stack acquisition, AiryScan mode) and image analysis using ImageJ-Win64 and Zen Blue3 software was performed.

Quantification of NET formation

To quantify the formation of NETs, microscopy images were obtained using a Zeiss LSM800 Confocal microscope with a 40x objective and 3x3 tiles acquisition. Three images per sample of three biological replicates were taken. To quantify NET formation by using NET-related signal dispersion of rRNA and DNA signal, ImageJ software was used, and a threshold (Triangle threshold) was applied as originally described (Zack, Rogers et al. 1977). Particles were analyzed with a ROI (region of interest) manager (size (micron^2): 100-infinity (pixel units); circularity 0.00-1.00) and average size and number of particles (ROIs) were assessed. In NETs, RNA and DNA signals showed up in a greater number and smaller size, making the usage of the ratio suitable as a measurement of NET-related signal dispersion. In the case

of using the DNA signal only to assess NET formation, ImageJ software was used to create a PNG image and a grid with 8x8 tiles was manually applied to the images. Tiles containing extracellular DNA structures were manually counted in a blinded manner as NET-positive tiles.

Live fluorescence microscopy of enzymatic digest of human NETs

500 µL of 1.6 x 10^6 cells/mL of human blood PMNs were seeded in a 4-well glass bottom microscopy cell culture dish (Greiner, 627871) and rested for 30 min before stimulation at 37°C and 5% CO_2 with PMA (600 nM) for 3 h. After stimulation, the medium was carefully removed and the cells were washed with PBS before adding fresh culture medium (RPMI culture medium without phenol red (Sigma-Aldrich, R7509) + 10% FBS (heat inactivated, sterile filtered, TH Geyer, 11682258)). Hoechst 33342 (Thermo Fisher, 1 µg/mL) to stain nuclear DNA and SYTO RNAselect Green fluorescent dye (Thermo Fisher, 50 µM) to stain naRNA was added to the cells, as well as RNase A (Thermo Fisher, EN0531; 100 µg/mL) or DNase I (Thermo Fisher, EN0521, 1 U/10 µL) was added between time point 0 and 5 min. Live cell imaging was performed using a Zeiss LSM800 Confocal microscope with a 63x objective and Z-stack acquisition, taking an image every 5 min for 30-60 min respectively. Image analysis and video creation was performed using ImageJ-Win64.

Click chemistry of primary, stem cell-derived PMNs and fluorescence microscopy

500 µL of 1.6 x 10^6 cells/ml of human stem cell-derived PMNs treated with 5-ethynyl uridine or left untreated were seeded in a 24-well plate containing poly-L-lysine-coated glass coverslips and rested for 30 min before stimulation with PMA (600 nM) at 37°C and 5% CO_2 for 12 h. After stimulation, the cells were washed and permeabilized with ice-cold acetone (Applichem, A1582.2500PE) 1:1 methanol (Honeywell, 32213-2.5L) for 5 min at RT. Subsequently, the click chemistry (reagents see Supplementary Table S4) labeling of endogenous RNA was performed as described (Presolski, Hong et al. 2011). Briefly, in a total volume of 500 µL, 2 µL of AF546-Azide, a pre-mixture of 1 mM $CuSO_4$ and 1.25 mM THPTA, 5 mM aminoguanidine-hydrochloride and 5 mM Na-ascorbate in PBS were added to the cells in a 24-well plate. The wells were sealed with plastic foil and incubated for 1 h at RT while shaking in the dark. For negative controls, 5-ethynyl uridine untreated cells incubated with complete click chemistry reagents and 5-ethynyl uridine treated cells incubated with PBS and AF546-Azide only were used. No significant signals were observed. After the incubation, the cells were washed three times for 5 min with PBS and counterstained with rRNA Y10b-AF647 (see Supplementary Table S3) at 1:50 in PBS for 2 h at RT in the dark. After repeated washing, the cells were incubated with Hoechst 33342 to stain nuclear DNA and mounted as described above. Imaging and analysis were performed as previously described.

Electron microscopy

For Electron microscopy, 500 µL of 1.6 x 10^6 cells/ml of human blood-derived PMNs were seeded in a 24-well plate containing coverslips which were pre-coated with 0.01 % poly-L-lysine (Sigma, A-005-C) for 15 min at 37°C. Cells were rested for 30 min at 37°C and 5% CO_2 and subsequently stimulated with 1200 nM PMA for 3 h. Afterwards, the cells were fixed in 2.5% glutaraldehyde in PBS for 1 h at room temperature followed by 4°C. Samples were post-fixed with 1% osmium tetroxide for 1 h on ice. Subsequently, samples were dehydrated in a graded ethanol series followed by critical point drying (CPD300, Leica Microsystems) with CO_2. Finally, the cells were sputter-coated with a 4 nm thick layer of platinum (CCU-010, Safematic) and examined with a field emission scanning electron microscope (Regulus 8230, Hitachi High Technologies) at an accelerating voltage of 3 kV. For antibody labeling, cells treated as described above were fixed in 4% formaldehyde in PBS for 1-2 hours at room temperature and 4°C overnight. After washing and blocking (0.2% gelatin in PBS) samples were incubated for 1 h at room temperature with rRNA Y10b as the primary antibody in blocking buffer and for 1 h at RT with goat anti-mouse antibodies coupled to 12 nm or 6 nm gold in blocking buffer (Jackson ImmunoResearch, code numbers 115-205-146 and 115-195-166, respectively). Samples labeled with 6 nm gold were further silver enhanced. Following immunolabeling, the samples were treated with 1% uranyl acetate for 5 min at RT, dehydrated and critical point dried as before. Samples were sputter-

coated with a 5 nm thick layer of carbon (CCU-010, Safematic) and analyzed in the SEM with an accelerating voltage of 5 kV.

Transient transfection of HEK293T cells

HEK293T cells were transiently transfected with the respective TLR8, TLR7, TLR9 and NF-κB reporter plasmids as described (Colak, Leslie et al. 2014) (see Supplementary Table S5 for plasmids) using X-tremeGENE™ HP DNA Transfection Reagent (Merck, 6366236001). A total amount of 5 x 10^4 cells/well were seeded in a 24-well plate one day prior to transfection. For the transfection of one well, 100 ng of the according TLR plasmid, 100 ng of the firefly luciferase NF-κB reporter and 10 ng *Renilla* luciferase control reporter was mixed in Opti-MEM™ Reduced Serum Medium (Thermo Fisher, 31985062) in a total volume of 50 µL. After 15 min incubation at RT, the transfection mix was added to the cells and the cells were incubated for 48 h. Prior to subsequent stimulation, the medium was changed to complete DMEM medium (Sigma, D5796-24X500ML), and the cells were incubated with the respective NET content stimuli and controls (R848 (2.5 µg/mL), TL8 (100 ng/mL), CpG (1.25 µM) + DOTAP (25 µg/mL), ssRNA (0.6 µg/mL) + DOTAP (20 µg/mL), Mock NETs + RNase inhibitor (1:50 dilution), PMA NETs (1:50 dilution), PMA NETs + RNase inhibitor (1:50)) for 18 h at 37°C and 5% CO_2. Supernatants were then removed, and the cells frozen briefly at -80 °C. Subsequently they were used for dual luciferase assay.

Dual luciferase reporter assay

The dual luciferase reporter assay for detection NF-κB activation after TLR transfection and subsequent stimulation was performed as described (Herster, Bittner et al. 2020). In brief, supernatants were removed from the cells after stimulation and 60 µL/well of 1X passive lysis buffer (E194A, Promega) was added. The plate was then incubated for 15 min at RT on the plate shaker and subsequently stored at −80 °C for at least 15 min to facilitate complete cell lysis. After thawing, the cell solution (60 µL) was transferred into a V-bottom 96-well plate and centrifuged for 10 min at 2500 rpm and 4 °C to pellet cell debris. Ten microliters of supernatant were then transferred into a white microplate and each condition was measured in triplicates using the FLUOstar OPTIMA device (BMG Labtech). Firefly and Renilla luciferase activity were determined using the Promega Dual luciferase kit. Both enzyme activities were measured for 12.5 s with 24 intervals of 0.5 s, respectively. The data was analyzed by calculating the ratio of the two measured signals, thereby normalizing each firefly luciferase signal to its corresponding Renilla luciferase signal. The ratios were represented as the relative light units (RLU) of NF-κB activation.

Extracellular bacterial killing of *S. aureus*

The killing assay of *S. aureus* with human PMNs was performed according to Brinkmann *et al*., 2004 (Brinkmann, Reichard et al. 2004). In brief, PMNs were seeded at a density of 2x10^6 cells/mL and incubated with PMA (600 nM) for 2 h at 37 °C. Afterwards, the medium was carefully replaced with serum-free culture medium, containing 2% heat-inactivated pooled human serum with cytochalasin D (10 µg/mL) and incubated further for 15 min before infection with bacteria. Cytochalasin D treatment did not affect NETs and this concentration was effective in blocking bacterial phagocytosis. To investigate whether naRNA of NETs was important in extracellular killing, samples were either treated with RNase A (Thermo Fisher, EN0531; 100 µg/mL) or DNase I (Thermo Fisher, EN0521; 1 U/10 µL) for 2 h during NET formation, or after NET formation during the 30 min bacterial killing process. Samples were centrifuged at 700 x g for 10 min and incubated at 37 °C and 5% CO_2 for 30 minutes. Bacterial killing was measured as percentages of control values (bacteria incubated alone in media without neutrophils).

In vivo analysis of naRNA DAMP effects

To investigate the effect of NETs with or without RNase inhibitors and the respective TLR signaling, 20 µL of NET content and the respective controls were injected into the ears of C57BL/6 and *Tlr13*$^{-/-}$ mice intradermally on day 0. Afterwards, as a measure of inflammation, the ear thickness was assessed using a manual caliper (0.01–10 mm, Peacock, Tokyo, Japan) until day 4.

Neutrophil infiltration *in vivo* fluorescence imaging

The *in vivo* experiment for investigating neutrophil infiltration was performed as described (Herster, Bittner et al. 2020). Briefly, LysM$^{EGFP/+}$ mice were injected intradermally with 20 µL of PMA or Mock NET content or respective controls. LysM$^{EGFP/+}$ mice were then anesthetized with inhalation isoflurane and *in vivo* fluorescence imaging was performed using the IVIS Lumina II imaging system (Caliper). EGFP fluorescence was measured using excitation (465 nm), emission (515–575 nm), and exposure time (0.5 s). Data are quantified as total radiant efficiency ([photons/s]/[µW/cm^2]) within a circular region of interest using Living Image software (Caliper).

Imiquimod model of psoriatic skin inflammation

To analyze the effect of RNA signaling in an *in vivo* model for psoriasis, the well-established imiquimod mouse model was used (Gilliet, Conrad et al. 2004). C57BL/6 and *Tlr13*$^{-/-}$ mice were used and, briefly, 70 µL (62.5 mg) of imiquimod (5%, Taro Pharmaceuticals Industries, Hawthorne, NY) was applied daily to both sides of a mouse ear for 5 consecutive days (day 0 to 4). Ear thickness was measured with a manual caliper (0.01–10 mm, Peacock, Tokyo, Japan) before imiquimod application. A day after the last application of imiquimod (day 5), full-thickness ear skin was excised with surgical scissors for histologic analysis.

ELISA

To measure cytokine release of BlaER-1, THP-1, N/TERT-1, NHEK, NK-92 MI, PBMCs and 3D human skin equivalent after stimulation with NET content and respective controls, ELISA Kits for hIL-8 (ELISA MAX™ Deluxe Set Human IL-8, Biolegend, 431504), hIL-6 (ELISA MAX™ Deluxe Set Human IL-6, Biolegend, 430504), IFN-γ (ELISA MAX™ Deluxe Set Human IFN-γ, Biolegend, 430104), and TNF (TNF alpha Human Uncoated ELISA Kit, Invitrogen, 88-7346-88) were used according to the manufacturer's instructions. Samples were assessed in triplicates.

qPCR analysis of IL-8 expression of 3D human skin equivalent

To investigate IL-8 expression of 3D human skin equivalent after stimulation with NET contents, qPCR analysis was performed. First, total RNA was isolated using the RNeasy Mini Kit (Qiagen, 74106) for animal tissues and cells. For cDNA preparation, the High-Capacity RNA-to-cDNA-Kit (Thermo Fisher, 4387406) was used according to the manufacturer's instructions. For the qPCR, the TaqMan™ system was used. Briefly, a master mix of TaqMan™ Universal Mastermix II (Thermo Fisher, 4440040) and TaqMan™ Gene Expression Assay (Thermo Fisher, 4448892) was prepared according to the manufacturer's instructions. For one reaction, 5.5 µL master mix and 4.5 µL of the respective cDNA (IL-8 and TBP) were mixed and the qPCR was run. Analysis in triplicates was performed using QuantStudio Real-Time-PCR software version 1.3 (Thermo Fisher).

Supplementary Tables

Supplementary Table 1: commercial TLR ligands and inhibitors; enzymes

Component	Company	Product no.
Cl-amidine	Merck	506282
CpG PTO 2006	TIB Molbiol	n/a, see Table S2
CU-CPT9a	Invivogen	inh-cc9a
DNase I	Thermo Fisher	EN0521
DNase inhibitor 50 mM EDTA	Thermo Fisher	EN0521
DOTAP	Roth	L787.2
Ionomycin	Sigma	I0634-1MG
LL37	Invivogen	tlrl-l37
LPS-EK (ultrapure)	Invivogen	tlrl-peklps
Nigericin	Invivogen	tlrl-nig
PMA	Invivogen	tlrl-pma
R848 (Resiquimod)	Invivogen	tlrl-r848
RNase A	Thermo Fisher	EN0531
RNase inhibitor	Promega	N2615
TL8-506	Invivogen	tlrl-tl8506

Supplementary Table 2: Nucleic acid TLR agonists

Component	Sequence	Backbone	Company
RNA40	5'GsCsCsCsGsUsCsUsGsUsUsGsUsGsUsGsAsCsUsC3'	Phosphorothioate	Eurogentec
CpG PTO 2006	5'TsCsGsTsCsGsTsTsTsTsGsTsCsGsTsTsTsTsGsTsCsGsTsT3'	Phosphorothioate	TIB

Supplementary Table 3: Antibodies and conjugation kit

Item	Fluorophore	Species	Isotype	Company	Product no.
Anti-hLL37	DyLight 550	Rabbit	IgG	LSBio	LS-B6696-500
DyLight 550 Conjugation Kit (Fast)	DyLight 550	-	-	Abcam	ab201800

Anti-rRNA (Y10b)	unconjugated	mouse	IgG_{2a} κ	Santa Cruz Biotechnology	sc-33678
Anti-rRNA (Y10b) Alexa Fluor® 647	AF647	mouse	IgG_{2a} κ	Santa Cruz Biotechnology	sc-33678 AF647
Anti-mouse IgG	AF647	Chicken	IgY	Thermo Fisher	A-21463
Hoechst 33342		-	-	Thermo Fisher	H21492
SYTO RNAselect Green fluorescent dye		-	-	Thermo Fisher	S32703

Supplementary Table 4: Click chemistry reagents

Reagent	Company	Product no.
AF546-Azide	Jena Bioscience	CLK-1283-1
Aminoguanidine-Hydrochloride	Merck	396494-25G
$CuSO_4$-click chemistry grade	Jena Bioscience	CLK-MI004-50.1
5-Ethynyluridine	Jena Bioscience	CLK-N002-10
Na-Ascorbate-click chemistry grade	Jena Bioscience	CLK-MI005-1G
THPTA (Tris((1-hydroxy-propyl-1H-1,2,3-triazol-4-yl)methyl)amine)	Jena Bioscience	CLK-1010-25

Supplementary Table 5: Plasmids used for HEK293T transfection

Plasmid name insert	Vector backbone	Insert
NF-κB reporter	pGL3	6x NF-κB response element
Renilla	pRL-TK	Renilla
hTLR7	pcDNA3.1 (+)	hTLR7
hTLR8	pcDNA3.1 (+)	hTLR8
hTLR9	pSEM-hTLR9	hTLR9

Supplementary Table 6: primers used for qPCR

Gene	Assay number
IL-8	Hs00174103_m1
TBP (housekeeper)	HS00427620_m1

Supplementary Table *7*: *10x Ammonium chloride erythrocyte lysis buffer*

Compound	Company	Product no.
1.54 M NH_4Cl	Roth	5470.1
100 mM $KHCO_3$	Fluka	60220
1 mM EDTA; pH 8	Thermo Fisher	15575020
dissolved in Ampuwa water	Fresenius Kabi	1833
pH adjusted to 7.3, sterile filtered (0.22 µm)		

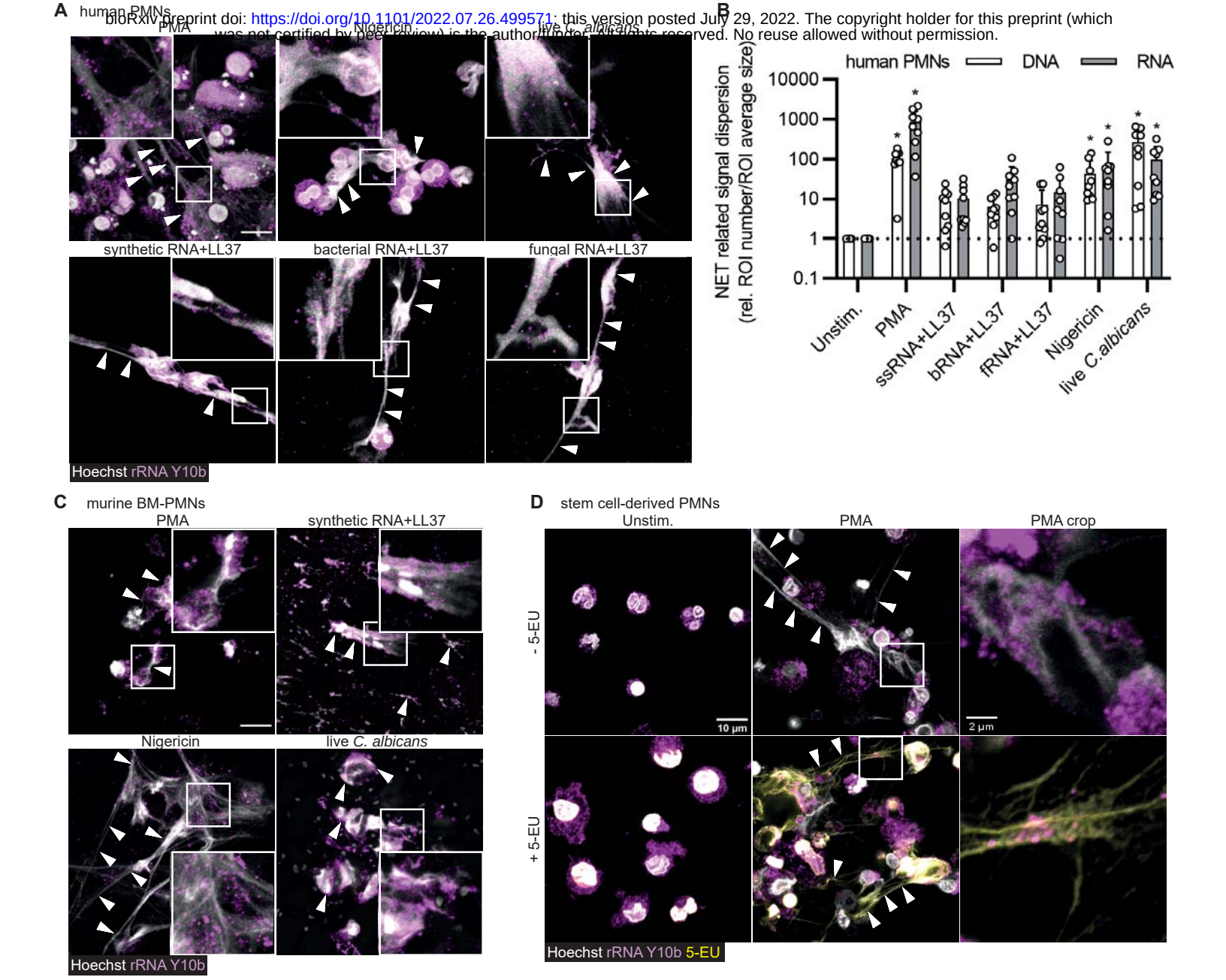

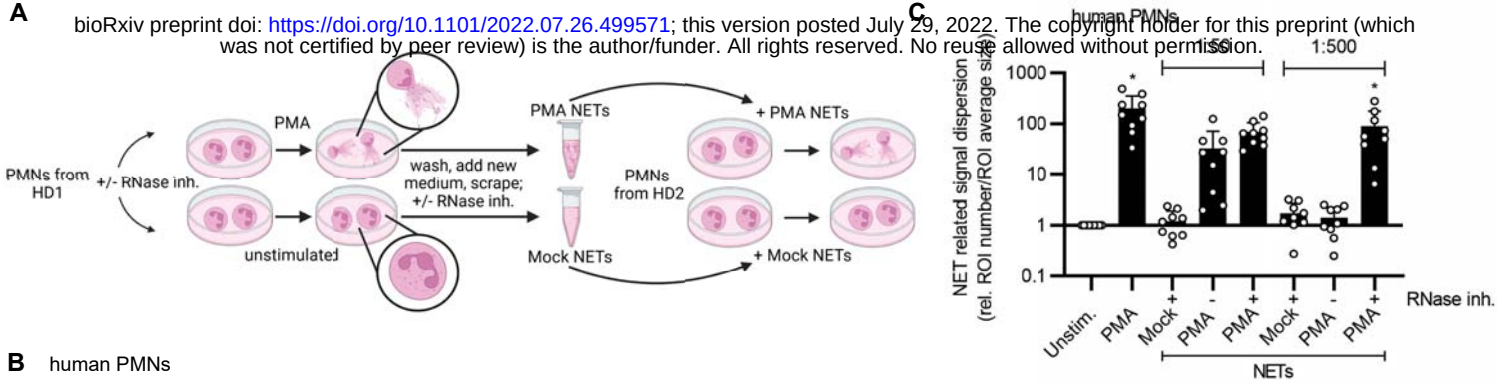

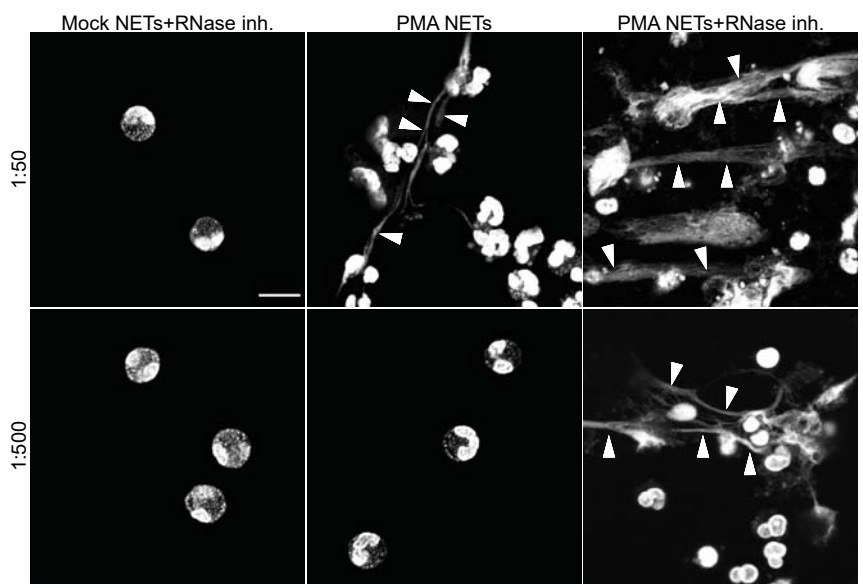

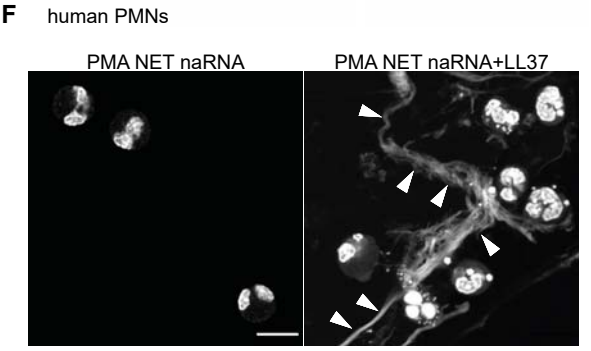

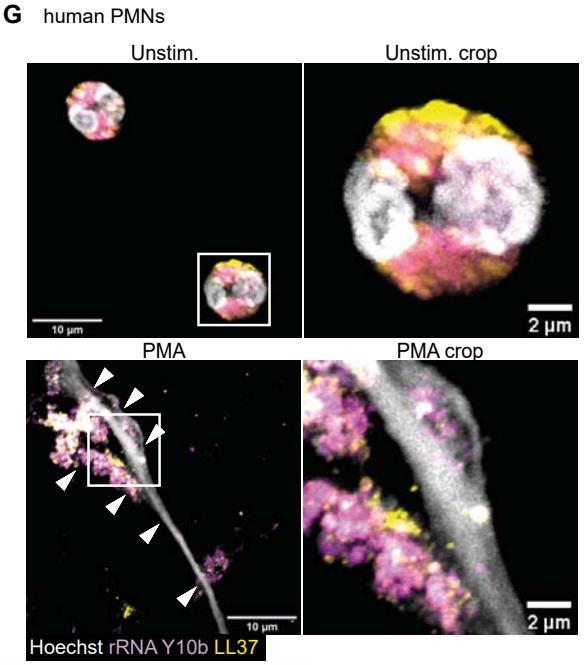

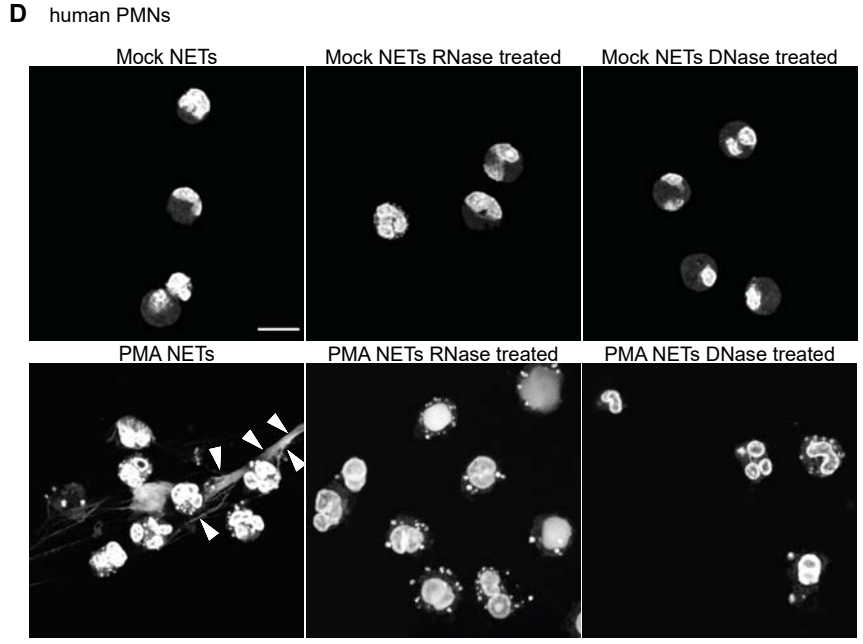

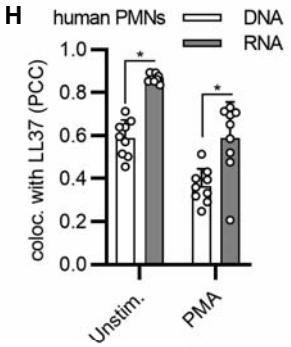

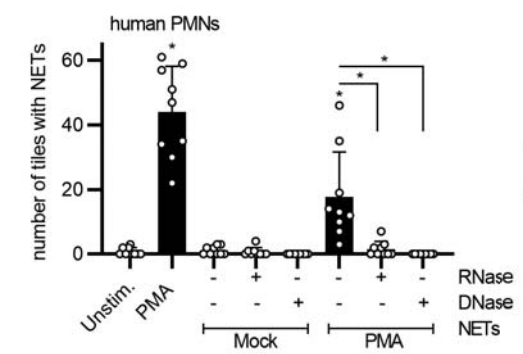

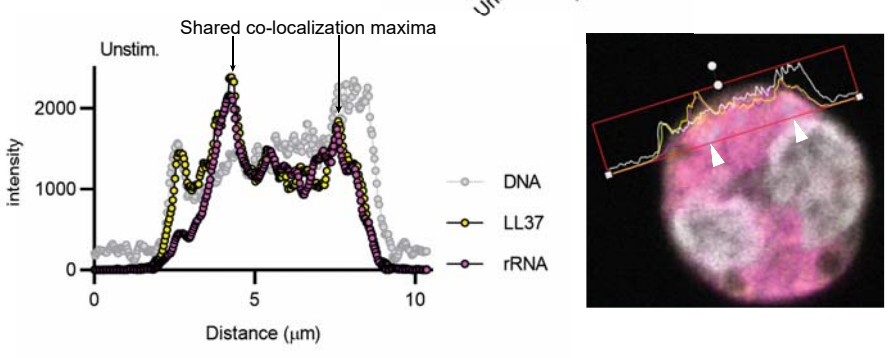

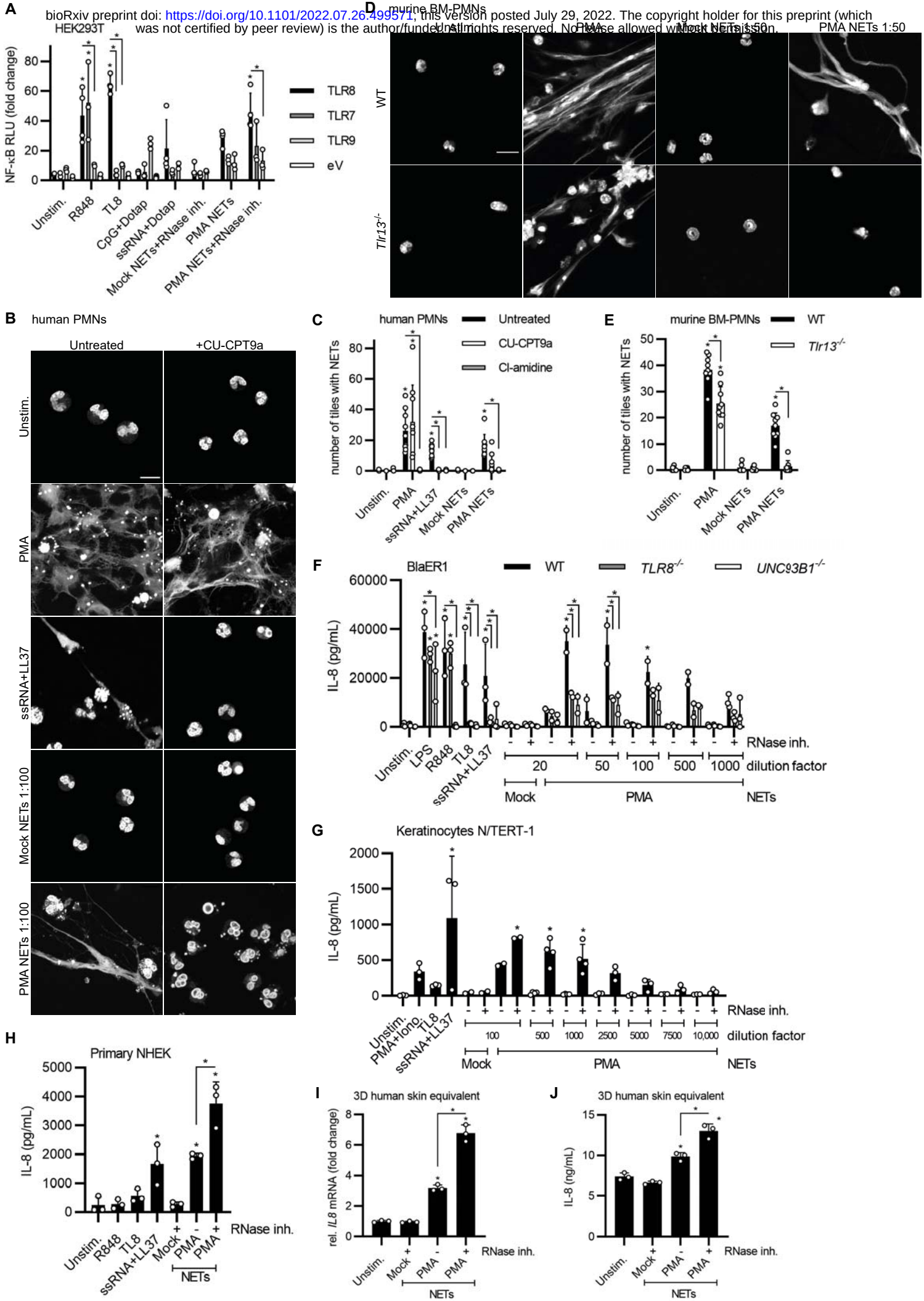

A

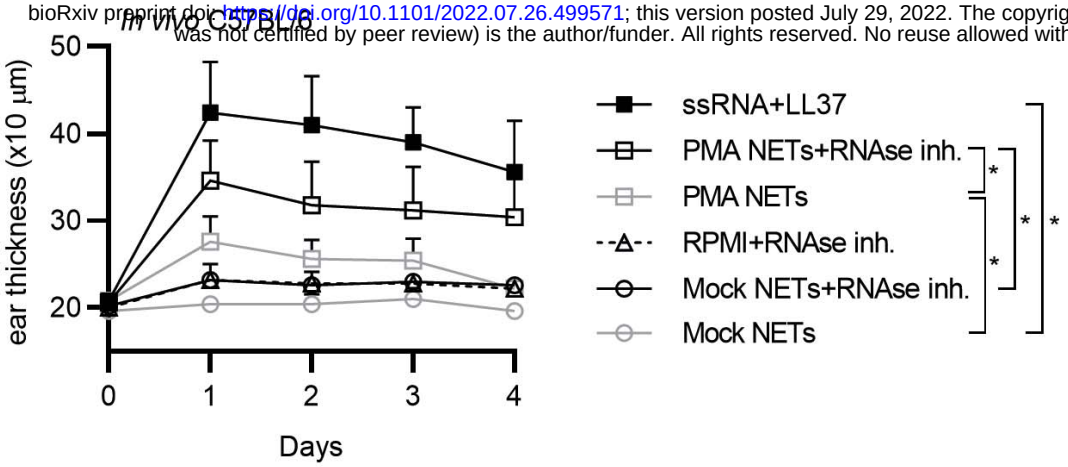

B

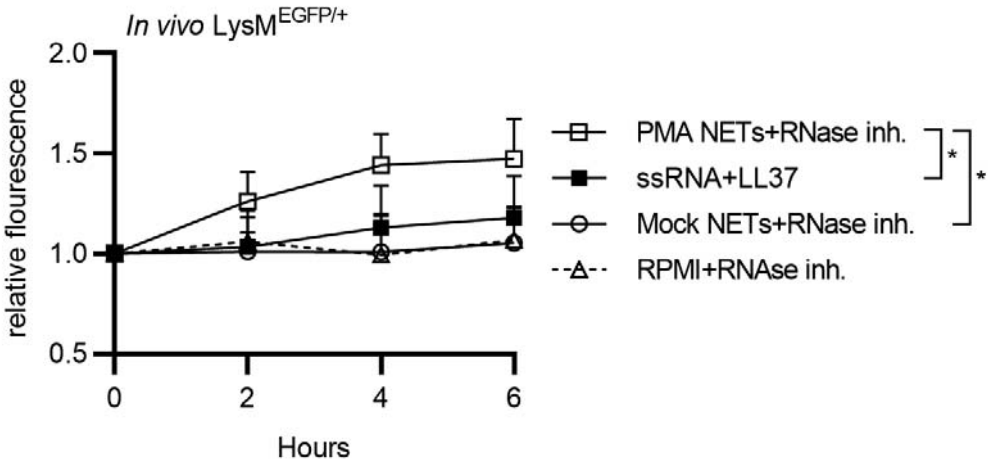

C

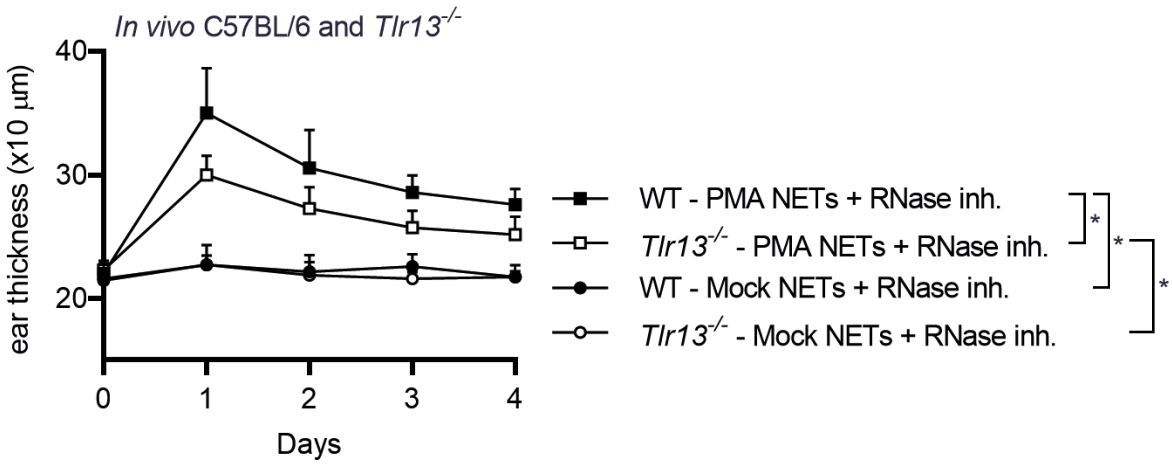

D